Mechanism of ozone loss under enhanced water vapour conditions in the mid-latitude lower stratosphere in summer

Sabine Robrecht[1], Bärbel Vogel[1], Jens-Uwe Grooß[1], Karen Rosenlof[2], Troy Thornberry[2,3], Andrew Rollins[2], Martina Krämer[1], Lance Christensen[4], and Rolf Müller[1]

[1]Forschungszentrum Jülich, Institute of Energy and Climate Research (IEK-7), Jülich, Germany
[2]NOAA Earth System Research Laboratory (ESRL) Chemical Sciences Division, Boulder, CO 80305 USA
[3]University of Colorado, Cooperative Institute for Research in Environmental Sciences, Boulder, CO 80309 USA
[4]California Institute of Technology, Jet Propulsion Laboratory, Pasadena, CA 91125 USA

Correspondence: Sabine Robrecht (sa.robrecht@fz-juelich.de)

Abstract. Water vapour convectively injected into the mid-latitude lowermost stratosphere could affect stratospheric ozone. The associated potential ozone loss process requires low temperatures together with elevated water vapour mixing ratios. Since this ozone loss is initiated by heterogeneous chlorine activation on liquid aerosols, an increase in sulphate aerosol surface area due to a volcanic eruption or geoengineering could increase the likelihood of its occurrence. However, the chemical mechanism of this ozone loss process has not yet been analysed in sufficient detail and its sensitivity to various conditions is not yet clear. Under conditions of climate change associated with an increase in greenhouse gases, both a stratospheric cooling and an increase in water vapour convectively injected into the stratosphere is expected. Understanding the influence of low temperatures, elevated water vapour and enhanced sulphate particles on this ozone loss mechanism is a key step in estimating the impact of climate change and potential sulphate geoengineering on mid-latitude ozone.

Here, we analyse the ozone loss mechanism and its sensitivity to various stratospheric conditions in detail. Conducting a box-model study with the Chemical Lagrangian Model of the Stratosphere (CLaMS), chemistry was simulated along a 7-day backward trajectory. This trajectory was calculated neglecting mixing of neighbouring air masses. Chemical simulations were initialized using measurements taken during the Study of Emissions and atmospheric Composition, Clouds and Climate Coupling by Regional Surveys (SEAC^{4}RS) aircraft campaign (2013, Texas), which encountered an elevated water vapour mixing ratio of 10.6 ppmv at a pressure level around 100 hPa. We present a detailed analysis of the ozone loss mechanism, including the chlorine activation, chlorine catalysed ozone loss cycles, maintenance of activated chlorine and the role of active nitrogen oxide radicals (NO_x). Focussing on a realistic trajectory in a temperature range from 197–202 K, a threshold in water vapour of 10.6 ppmv has to be exceeded and maintained for stratospheric ozone loss to occur. We investigated the sensitivity of the water vapour threshold to temperature, sulphate content, inorganic chlorine (Cl_y), inorganic nitrogen (NO_y) and inorganic bromine (Br_y). The water vapour threshold is mainly determined by the temperature and sulphate content. However, the amount of ozone loss depends on Cl_y, Br_y and the duration of the time period over which chlorine activation can be maintained. NO_y affects both the potential of ozone formation and the balance between reactions yielding chlorine activation and -deactivation, which determines the water vapour threshold. Our results show that in order to deplete ozone, a chlorine activation time of 24 to 36 hours for conditions of the water vapour threshold with low temperatures must be maintained. A maximum ozone

loss of 9% was found for a 20 ppmv water vapour mixing ratio using North American Monsoon (NAM) tropopause standard conditions with a chemical box-model simulation along a realistic trajectory. For the same trajectory, using observed conditions (of 10.6 ppmv H_2O), the occurrence of simulated ozone loss was dependent on the sulphate amount assumed. Detailed analysis of current and future possibilities is needed to assess whether enhanced water vapour conditions in the summertime mid-latitude lower stratosphere lead to significant ozone loss.

1 Introduction

The impact of water vapour convectively injected into the lowermost stratosphere on the mid-latitude ozone layer is a matter of current debate (Anderson et al., 2012, 2017; Ravishankara, 2012; Schwartz et al., 2013). While Anderson et al. (2012) focused on the heterogeneous chemistry of cold liquid sulfate aerosol, earlier studies have focussed on the influence of cirrus clouds on ozone chemistry in the lowermost stratosphere (Borrmann et al., 1996, 1997; Solomon et al., 1997; von Hobe et al., 2011). Anderson et al. (2012) proposed a potential ozone depletion in the mid-latitude stratosphere in summer on liquid sulphate aerosols under conditions of enhanced water vapour and low temperatures. They proposed this chemical ozone loss to be initiated through heterogeneous chlorine activation and to be driven by catalytic ozone loss cycles related to ozone loss known from polar regions in early spring (e.g. Grooß et al., 2011; Solomon, 1999; Vogel et al., 2011). Here, we present a detailed analysis of this ozone loss mechanism and an extensive investigation of its sensitivity to a variety of conditions.

In the bulk and on the surface of cold condensed stratospheric particles, such as binary H_2SO_4/H_2O solutions, ternary solutions, NAT (Nitric Acid Trihydrate) and ice particles (e.g. Spang et al., 2018), inactive chlorine species (HCl, $ClONO_2$) can be converted to active chlorine (ClO_x=Cl+ClO+2 × Cl_2O_2+2 × Cl_2) through the heterogeneous reactions R1, R2 and R3 (Solomon et al., 1986; Prather, 1992; Crutzen et al., 1992) and the subsequent photolysis of Cl_2 and HOCl.

$$ClONO_2 + HCl \xrightarrow{het.} HNO_3 + Cl_2 \quad \text{(R1)}$$

$$ClONO_2 + H_2O \xrightarrow{het.} HNO_3 + HOCl \quad \text{(R2)}$$

$$HCl + HOCl \xrightarrow{het.} H_2O + Cl_2 \quad \text{(R3)}$$

The heterogeneous reactions R1 and R2 drive the conversion of active nitrogen-oxides (NO_x=NO + NO_2 + NO_3 + 2 × N_2O_5) into HNO_3. After chlorine activation, catalytic ozone loss cycles can occur, such as the ClO-dimer-cycle (Molina and Molina, 1987) and the ClO-BrO-cycle (McElroy et al., 1986). These cycles are responsible for the rapid ozone loss observed in Antarctic spring (e.g. Solomon, 1999). A third cycle with ClO and HO_2 (see Sec. 3) proposed by Solomon et al. (1986) would be expected to play a role in ozone loss in the mid-latitude lower stratosphere (e.g. Daniel et al., 1999; Ward and Rowley, 2016). This cycle was originally proposed as an ozone depleting cycle in the Antarctic lower stratosphere, but for polar ozone destruction, this cycle turned out to be of minor importance (Solomon, 1999).

Under the very dry conditions in the polar stratosphere, very low temperatures (below ∼195 K) are required for heterogeneous chlorine activation through reactions R1–R3 (Solomon, 1999; Shi et al., 2001). An enhancement of water vapour above background values would allow chlorine activation at higher temperatures (200–205 K) (Drdla and Müller, 2012), which led to

the hypothesis that chlorine activation and subsequent ozone loss could occur at mid-latitudes in summer in the lowermost stratosphere (Anderson et al., 2012, 2017; Anderson and Clapp, 2018). The aim of our study is to investigate for a variety of conditions by how much water vapour has to be enhanced for chlorine activation to occur at these higher temperatures.

An enhanced stratospheric sulphate aerosol content increases heterogeneous chlorine activation by increasing the surface area of the condensed particles (Drdla and Müller, 2012; Solomon, 1999). As an example, the aerosol surface area density in the lower stratosphere ranges between ∼0.5 and 1.5 $\mu m^2 cm^{-3}$ under non-volcanic conditions (Thomason and Peter, 2006), while the perturbation of Mt. Pinatubo yielded peak values of more than 40 $\mu m^2 cm^{-3}$ (Thomason et al., 1997). In the stratosphere, water vapour increases with altitude, primarily due to methane oxidation (LeTexier et al., 1988; Rohs et al., 2006). The upper branch of the Brewer Dobson circulation (BDC) transports higher stratospheric water vapour mixing ratios down to lower altitudes at mid to high latitudes, and this air mixes with the low water vapour containing air from the tropics that has moved poleward in the lower branch of the BDC (e.g. Brewer, 1949; Randel et al., 2004; Poshyvailo et al., 2018), giving typical mid-latitude lowermost stratosphere values of 2–6 ppmv H_2O. However, above North America in summer,enhanced water vapour mixing ratios of 10–18 ppmv at an altitude of ∼16.5 km (380 K potential temperature, ∼ 100 hPa) (Smith et al., 2017) have been observed, which were connected with deep convective storm systems penetrating the tropopause (Homeyer et al., 2014; Herman et al., 2017; Smith et al., 2017). These convective overshooting events can transport ice crystals into the lowermost stratosphere, where the ice evaporates leading to a local enhancement of water vapour (Hanisco et al., 2007; Schiller et al., 2009; Herman et al., 2017).

As greenhouse gases increase in the atmosphere, models predict that more water may be convectively transported into the stratosphere (Trapp et al., 2009; Klooster and Roebber, 2009). This increases the probability that the ozone loss process proposed by Anderson et al. (2012) will occur, especially in the case of an additional enhancement of stratospheric sulphate particles caused by volcanic eruptions or sulphate geoengineering. The occurrence of this ozone loss process requires halogens to be present, which are decreasing in the stratosphere due to the Montreal Protocol and its amendments and adjustments (WMO, 2018). However, for assessing the impact of geoengineering on the ozone layer, also the impact of very short lived halogens needs to be taken into account (Tilmes et al., 2012). For estimating the impact of both climate change and a possible sulphate geoengineering on the mid-latitude ozone layer, it is necessary to consider the influence of enhanced water vapour and sulphate content on mid-latitude ozone chemistry in the lowermost stratosphere in detail.

In the study by Anderson et al. (2012), a range of initial mixing ratios for HCl and $ClONO_2$ with rather high concentrations of 850 pptv HCl and 150 pptv $ClONO_2$ was assumed. Here, we investigate ozone loss in mid-latitude summer based on measurements from flights by the NASA ER-2 aircraft during the Studies of Emissions and Atmospheric Composition, Clouds and Climate Coupling by Regional Surveys (SEAC^{4}RS) campaign, which was based in Houston, Texas in 2013 (Toon et al., 2016). Conducting box-model simulations with the Chemical Lagrangian Model of the Stratosphere (CLaMS, McKenna et al., 2002a, b), the ozone loss mechanism is analysed in greater detail. The model setup is described in Section 2. In Sec. 3, the chlorine activation step, catalytic ozone loss cycles and the maintenance of activated chlorine levels in the mid-latitude stratosphere are investigated in detail. The sensitivity of this mechanism to water vapour, sulphate content, temperature, Cl_y mixing ratio (Cl_y=HCl+$ClONO_2$+ClO_x), reactive nitrogen (NO_y=NO_x+HNO_3) and inorganic bromine (Br_y) is explored in Sec. 4. Case

studies, which extend the simulated time period and assume conditions based on SEAC^{4}RS measurements as well as conditions used in the study of Anderson et al. (2012), further illustrate these sensitivities in Sec. 5.

2 Model setup

The simulations presented here were performed with the box-model version of CLaMS (McKenna et al., 2002a, b). Stratospheric chemistry is simulated based on a setup used in previous studies (Grooß et al., 2011; Müller et al., 2018; Zafar et al., 2018) for single air parcels along trajectories including diabatic descent and neglecting mixing between neighbouring air masses. A full chemical reaction scheme comprising gas phase and heterogeneous chemistry is applied using the SVODE-solver (Brown et al., 1989). Chemical reaction kinetics are taken from Sander et al. (2011), photolysis rates are calculated for spherical geometry (Becker et al., 2000), and heterogeneous reaction rates for R1–R3 were calculated based on the the study of Shi et al. (2001). For heterogeneous particle formation, the initial liquid aerosol number density (N_0=10.0 cm^{-3}), the standard deviation of the logarithmic normal distribution of the particle size (σ=1.8), and the gas phase equivalent of the amount of sulfuric acid in the aerosol (for chosen values see Tab. 1) are set prior to the simulation. The gas phase equivalent is used to calculate the density of liquid particles as described in the study of Shi et al. (2001) (binary solutions) and Luo et al. (1996) (ternary solutions). Particle size and surface area densitiy are calculated based on the density of liquid particles, the areosol number density, and the standard deviation. In contrast to the setup in Grooß et al. (2011), Müller et al. (2018) and Zafar et al. (2018), only formation of liquid particles (both binary H_2O/H_2SO_4 and ternary $HNO_3/H_2O/H_2SO_4$ solutions) is allowed (i.e. no NAT or ice particles are formed in this model setup) to enable a better comparability with the studies of Anderson et al. (2012, 2017) and Anderson and Clapp (2018). Note that this is also different from the study of Borrmann et al. (1996, 1997), who investigated lowermost stratospheric ozone chemistry on cirrus clouds.

2.1 Measurements

The box model simulations were initialized using water vapour, ozone and CH_4 measurements taken during the SEAC^{4}RS aircraft campaign (more information on the chemical initialization is provided in Section 2.3). It was based in Houston, Texas, and took place during August and September 2013 (Toon et al., 2016). One aim of this campaign was to investigate the impact of deep convective clouds on the water vapour content and the chemistry in the lowermost stratosphere. We initialized the model using measurements taken on 8 August 2013 by the Harvard Lyman-α photofragment fluorescence hygrometer (HWV, Weinstock et al., 2009), which flew on the NASA ER-2 high altitude research aircraft. Ozone was initialized in our simulations using O_3 measurements from the National Oceanic and Atmospheric Administration (NOAA) UAS-O_3-instrument (Gao et al., 2012). Initial Cl_y and NO_y were determined using tracer-tracer correlations (for more informations see Sec. 2.3) based on methane measurements with the Harvard University Picarro Cavity Ring down Spectrometer (HUPCRS) (Werner et al., 2017).

2.2 Trajectories

Diabatic trajectories were calculated using wind and temperature data from the ERA-Interim reanalysis (Dee et al., 2011) with $1^\circ \times 1^\circ$ resolution provided by the European Centre for Medium-Range Weather Forecasts (ECMWF). The vertical velocities were calculated from the total diabatic heating rates derived from ERA-Interim data (Ploeger et al., 2010). Trajectories (7-day forward and backward) were initialized at locations during SEAC^{4}RS where stratospheric water vapour was over 10 ppmv.

A selected example of calculated trajectories is shown in Fig. 1. This trajectory was chosen for the chemical analysis, because its initial conditions exhibited enhanced water vapour relative to the overall background, low temperatures and enhanced Cl_y (higher than for comparable water vapour and temperature conditions). Cl_y was calculated from tracer-tracer correlations (see Sec. 2.3). This trajectory is then most suitable for the occurrence of the mechanism proposed by Anderson et al. (2012). In the left panel, a backward trajectory is presented in the range of -7 to 0 days from the time of measurement (red line) and a forward trajectory in the range from 0 to 7 days. In the right panel, the location of the measurement is shown by a red square.

The shown trajectories (Fig. 1, a forward and a backward trajectory) are based on measurements on 8 August 2013 during the SEAC^{4}RS campaign. With a potential temperature of 380 to 390 K, these trajectories are above the tropopause of $\sim$366 K (Fig. 1 left, grey line), deduced from the temperature profile measured during the flight. Both, the forward and backward trajectories stay in the region of the North American continent. For the SEAC^{4}RS campaign, the temperature range of the backward trajectory varies between 197 and 202 K and the forward trajectory exhibits increasing temperatures. In addition, we considered trajectories based on other SEAC^{4}RS measurements with enhanced water vapour, however most of them exhibit higher mean temperatures of at least 200 K. Since low temperatures are expected to push stratospheric ozone depletion in mid-latitudes (Anderson et al., 2012) due to faster heterogeneous chemical reactions and thus faster chlorine activation, the SEAC^{4}RS backward trajectory (Fig.1, day -7 to 0) is selected here as the standard trajectory. This trajectory is used to analyse the chemical mechanisms affecting lower stratospheric ozone under various water vapour conditions, and to explore the sensitivity of these processes to different initial conditions.

2.3 Initialization

Important trace gases for ozone chemistry – O_3, Cl_y and NO_y – are initialized based on measurements during the SEAC^{4}RS aircraft campaign over North America (see Sec. 2.1). Ozone and water vapour were measured directly during the aircraft campaign, Cl_y and NO_y are inferred from tracer-tracer correlations using CH_4 measured on the aircraft employed. The initialization of all further trace gases except of water vapour were taken from the full chemistry 3D-CLaMS simulation (Vogel et al., 2015, 2016) for summer 2012 at the location of the measurement. Chemistry was initialized 7 days before the measurement. However, this time shift does not affect the sensitivities and the mechanism investigated here, because the trace gases Cl_y and NO_y were initialized based on measured CH_4 mixing ratios, which are not significantly changing during a 7-day box-model simulation.

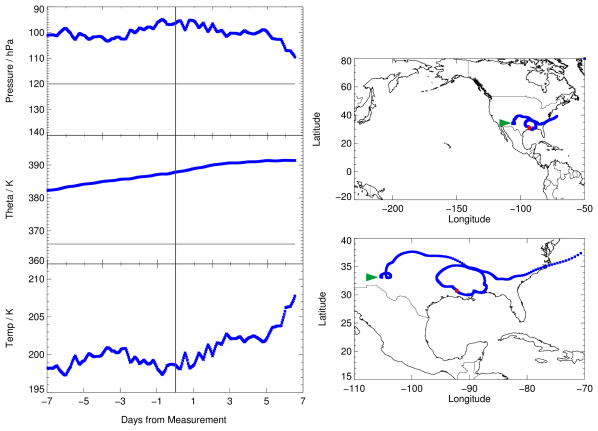

Figure 1. Pressure, potential temperature, temperature and location of the selected 7-day trajectories (forward and backward) calculated based on measurements with enhanced water vapour during the SEAC^{4}RS aircraft campaign. In the left panels, the grey line marks the approximate tropopause altitude, deduced from the temperature profile measured during the flight. The red line (left panel) marks the time of measurement and red squares (right panels) mark the location of the measurement. For the right panels, the bottom panel exhibits a zoom from the top panel and the begin of the backward-trajectory (1 August) is marked by a green arrow.

2.3.1 Standard case

In the standard case, the initial values of O_3, Cl_y and NO_y are determined based on an observation with an enhanced water vapour content of 10.6 ppmv (measured by the HWV-instrument) from the SEAC^{4}RS (Toon et al., 2016) aircraft campaign. A gas phase equivalent mixing ratio for background sulphuric acid (H_2SO_4) of 0.20 ppbv is assumed. Initial CO (49.6 ppbv) is taken from the 3D-CLaMS simulation (Vogel et al., 2015), which is higher than the measured value of 34.74 ppbv (measured by the HUPCRS instrument). Simulations assuming the measured CO mixing ratio showed only a minor difference to the results presented here. The initial values for the main trace gases for the standard case are summarized in Table 1. Note, in the 3D-CLaMS simulation, the mixing ratios of HCl (131 ppt, CLaMS), O_3 (206 ppb, CLaMS) and HNO_3 (354 ppt, CLaMS) are at the location of the SEAC^{4}RS measurement lower than in the standard initialization (see Tab. 1).

Since Cl_y and NO_y were not measured during the SEAC^{4}RS ER2-flights in the lowermost stratosphere, values for Cl_y and NO_y are calculated through tracer-tracer correlations (Grooß et al., 2014, see Appendix C for equations) based on a SEAC^{4}RS CH_4 measurement (of 1.776 ppmv) on 8 August 2013. The Cl_y-CH_4 correlation was calculated from measurements of the Airborne Chromatograph for Atmospheric Trace Species (ACATS) during flights of the ER-2 aircraft and from measurements by the cryogenic whole air sampler of the university of Frankfurt (on board of the TRIPLE balloon gondola) during balloon flights at mid and high latitudes in the year 2000 (Grooß et al., 2002). Between the year 2000 and 2013 stratospheric CH_4 increased and Cl_y decreased. Hence, the change of both lowermost stratospheric CH_4 and Cl_y has to be taken into account when using this tracer-tracer correlation. The increase in CH_4 was estimated to be equivalent to the growth rate for tropospheric CH_4. This growth rate was calculated to be 45.8 ppbv from the year 2000 to 2013 by determining and adding every annual mean

of the tropospheric CH_4 growth rate given in GHG Bulletin (2014). Subtracting this increase of CH_4 from the measured CH_4 mixing ratio yields an CH_4 equivalent for the year 2000. From the CH_4 equivalent, an equivalent Cl_y mixing ratio for the year 2000 was calculated using the tracer-tracer correlation (Grooß et al., 2014). The annual decrease of Cl_y is assumed to be 0.8% (WMO, 2014) from the year 2000 to 2013, and thus the initial Cl_y is calculated to be 156 ppt. Since most Cl_y is deactivated in the mid-latitude lowermost stratosphere, the initial mixing ratio of ClO_x species is assumed to be zero. A simulation assuming a ClO mixing ratio of 1% of total Cl_y, does not yield a significant difference to our standard case.

Initial NO_y was calculated through a N_2O correlation. Since no N_2O was measured on the ER2-flights during SEAC^{4}RS, stratospheric N_2O was first estimated through a methane correlation (Grooß et al., 2002), which is based on measurements from the year 2000. Hence, the equivalent CH_4 mixing ratio for the year 2000 (see above) was used to calculate an N_2O equivalent. Considering an estimated increase in N_2O of 10.4 ppbv from 2000 to 2013, which was determined in the same way as the CH_4 change (GHG Bulletin, 2014), the N_2O mixing ratio related to the time of the measurement in 2013 was calculated. Afterwards NO_y is calculated with a correlation from Grooß et al. (2014) to be 782.9 ppt.

This standard case initialization is shown in Table 1. Because of the uncertain conditions in convective overshooting plumes, sensitivity box-model simulations are conducted. Furthermore, testing the impact of various parameters on chemical ozone loss is intended to yield a better understanding of the balance between stratospheric ozone production and ozone loss, which is a key aspect for potential mid-latitude ozone depletion. The assumed water vapour content in a simulation is varied from 5 to 20 ppmv. In addition, simulations assuming the same water vapour range and a constant temperature in a range from 195–220 K are conducted assuming sulphate background conditions with a gas phase equivalent of 0.20 ppbv and 10×enhanced sulphate (2.00 ppbv) for illustrating the dependence of ozone loss on water vapour and temperature. Furthermore, sensitivity simulations are conducted, assuming 80% Cl_y, 80% NO_y or 50% Br_y, and a standard case simulation along a 19-day trajectory is calculated.

2.3.2 Case of high Cl_y

Simulations conducted assuming high Cl_y and NO_y concentrations taken from Fig. 2 in Anderson et al. (2012) are referred to as "Case of high Cl_y", which constitutes a worst case scenario. In the case of high Cl_y, HNO_3 is determined as 1.19 ppbv assuming the same ratio for HNO_3 (63% of total NO_y) and NO+NO_2 (37% of total NO_y) as in the standard case. An overview of the important trace gases in the initialization is given in Tab. 1. The results of the case initialized with high Cl_y are compared with the results obtained from standard case simulations.

3 Mid-latitude ozone chemistry

Mid-latitude ozone chemistry in the lowermost stratosphere depends on water vapour abundance and temperature. This study focuses on the water vapour dependence of stratospheric ozone chemistry by analysing chemical processes occurring in a box-model simulation along a realistic trajectory in the temperature range from 197-202 K under several water vapour conditions. In Figure 2, the mixing ratio of ozone, ClO_x and NO_x is shown for two simulations assuming 5 ppmv (dashed line) and 15 ppmv

Table 1. Mixing ratios and sources used for initialization of relevant trace gases. The standard initialization is based on SEAC^{4}RS measurements. Cl_y and NO_y values were determined based on tracer-tracer correlations (see Sec. 2.3.1). The high Cl_y case is based on Fig. 2 from Anderson et al. (2012). Initial mixing ratios of ClO_x species were assumed to be zero for all cases.

	Standard case			Case of high Cl_y	
Species	Value	Source	Sensitivity simulation	Value	Source
O_3	303.2 ppbv	UAS-O_3		303.2 ppbv	UAS-O_3
CH_4	1.76 ppmv	CLaMS-3D		1.76 ppmv	CLaMS-3D
CO	49.6 ppbv	CLaMS-3D		49.6 ppbv	CLaMS-3D
Cl_y	156 pptv	tracer corr.	80% Cl_y	1.00 ppbv	Anderson et al. (2012)
HCl	149.5 pptv	tracer corr.		850 pptv	Anderson et al. (2012)
$ClONO_2$	6.2 pptv	tracer corr.		150 pptv	Anderson et al. (2012)
NO_y	782.9 pptv	tracer corr.	80% NO_y	1.89 ppbv	
HNO_3	493.2 pptv	tracer corr.		1.19 ppbv	see section 2.3.2
NO	144.8 pptv	tracer corr.		325 pptv	Anderson et al. (2012)
NO_2	144.8 pptv	tracer corr.		375 pptv	Anderson et al. (2012)
Br_y	6.9 pptv	CLaMS-3D	50% Br_y	6.9 pptv	CLaMS-3D
H_2O	5–20 ppmv		5–20 ppmv	5–20 ppmv	
H_2SO_4	0.2 ppbv		0.6 ppbv, 2.0 ppbv	0.2 ppbv, 0.6 ppbv	
Temperature		standard trajectory	const. temp (195–220 K)		standard trajectory

(solid line) H_2O. These water vapour mixing ratios are chosen, because they are clearly in the regime of the low water vapour background (5 ppmv) of the lower mid-latitude stratosphere and of enhanced water vapour (15 ppmv) as it can be reached through convective overshooting events. For the low water vapour (5 ppmv) case, net ozone formation occurs, the ClO_x mixing ratio remains low and the NO_x mixing ratio high. In contrast, assuming a water vapour mixing ratio of 15 ppmv, ozone depletion occurs, accompanied by a decrease in NO_x and coupled with chlorine activation as indicated by the increasing ClO_x mixing ratio. The sensitivity to variations in water vapour conditions on stratospheric ozone is tested here by conducting simulations with standard conditions but varying the assumed water vapour mixing ratio from 5 to 20 ppmv in varying increments, with the resolution increased near the changeover from ozone production to destruction.

In Figure 3, the ozone values reached at the end of the 7-day simulation (final ozone, blue squares) are plotted as a function of the assumed water vapour mixing ratio. The initial ozone value, of 303.2 ppbv, is shown by the grey line. Blue squares lying above that line are cases with ozone production, those lying below that line are cases with ozone destruction. The decrease of final ozone with higher water vapour mixing ratios is related to chlorine activation. The time until chlorine activation occurs in this simulation is plotted in Fig. 3 as violet triangles, assuming that chlorine activation occurs when the ClO_x mixing ratio exceeds 10% of total Cl_y (Drdla and Müller, 2012). Shown is the time when chlorine activation first occurs in the model. Since the ClO_x/Cl_y ratio is dependent on the diurnal cycle, the 24-hours mean value of the ClO_x mixing ratio was used to determine

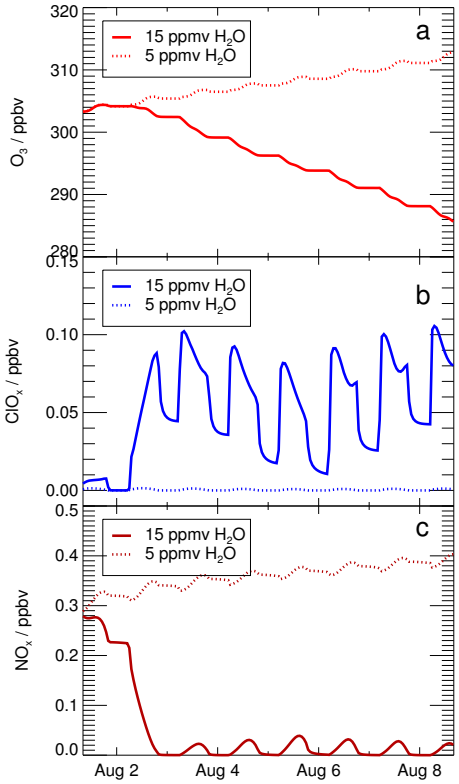

Figure 2. Volume mixing ratio of O_3 (a), ClO_x (b) and NO_x (c) during a simulation with 15 ppmv H_2O and 5 ppmv H_2O. These water vapour mixing ratios are chosen, because they are clearly in the regime of low (5 ppmv) and elevated (15 ppmv) water vapour. The x-axis ticks refer to 00:00 local time (06:00 UTC).

the chlorine activation time. For low water vapour mixing ratios, no chlorine activation time is plotted, because no chlorine activation occurs. For chlorine activation to occur, a threshold in water vapour has to be reached. Here, we determine the lowest water vapour mixing ratio at which chlorine activation occurs as water vapour threshold (marked by a blue arrow in Fig. 3). In our standard case, this threshold is reached at a water vapour mixing ratio of 10.6 ppmv. Between 10.6 and 11.8 ppmv H_2O, chlorine activation leads not to an ozone destruction during the 7-day simulation. For 10.6 to 11.2 ppmv H_2O, chlorine only remains activated for up to 28 h, because of increasing temperatures, and almost no impact on final ozone is observable. By 12.0 ppmv of water vapour, chlorine activation yields ozone destruction within the 7-day simulation. Near the water vapour threshold, the activation time is 24 to 36 hours and it decreases with increasing water vapour mixing ratios. It requires 5 hours at 20 ppmv H_2O. The shorter the chlorine activation time, the longer activated chlorine exists during the simulation yielding greater ozone depletion. The processes yielding ozone depletion at high water vapour conditions as well as ozone formation at

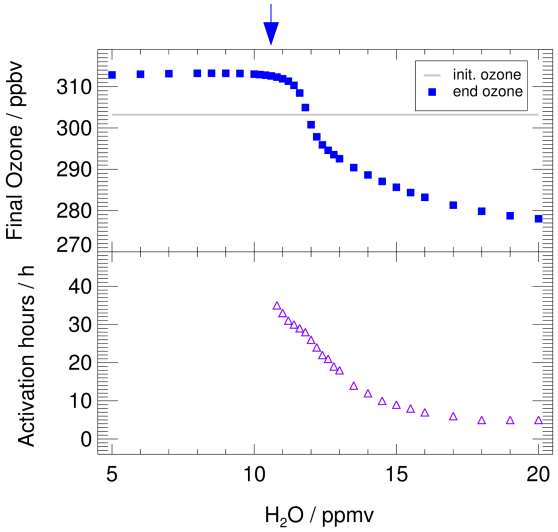

Figure 3. Impact of the water vapour content on the ozone mixing ratio (final ozone, blue squares) reached at the end of the 7-day simulation along the standard trajectory and assuming standard conditions. The initial ozone amount is marked by the grey line. The arrow marks the water vapour threshold, which has to be exceeded for chlorine activation at standard conditions to occur. In the bottom panel, violet triangles show the time until chlorine activation occurs. For low water vapour mixing ratios no chlorine activation occurs.

low water vapour are analysed in detail in the subsequent sections. For this investigation we use the simulated reaction rates for each chemical reaction along the course of the calculation. For high water vapour mixing ratios the roles of both chlorine activation and a decrease in the NO_x mixing ratio (Fig. 2) are discussed.

3.1 Ozone formation at low water vapour mixing ratios

At water vapour mixing ratios up to 11.8 ppmv, net ozone formation occurs during the 7-day simulation (see Fig. 3). This ozone formation is mainly driven by the photolysis of O_2. Additionally the "Ozone Smog Cycle" (Haagen-Smit, 1952) known from tropospheric chemistry can yield ozone formation in the lower stratosphere (Grenfell et al., 2006; Grooß et al., 2011).

$$OH + CO \rightarrow CO_2 + H \quad \text{(R4)}$$

$$H + O_2 + M \rightarrow HO_2 + M \quad \text{(R5)}$$

$$HO_2 + NO \rightarrow NO_2 + OH \quad \text{(R6)}$$

$$NO_2 + h\nu \rightarrow NO + O(^3P) \quad \text{(R7)}$$

$$O_2 + O(^3P) + M \rightarrow O_3 + M \quad \text{(R8)}$$

$$\text{net: } CO + 2\,O_2 \rightarrow CO_2 + O_3 \quad \textbf{(C1)}$$

The rate of this cycle is determined by reaction R4 at low water vapour mixing ratios, and its net reaction is the oxidation of CO. The ozone formation through this cycle contributes around 40% to the total ozone formation at 5 ppmv in our box model standard simulation. Hence, the ozone formation which occurs in the simulations assuming low water vapour mixing ratios is due to both the photolysis of O_2 and cycle **C1**.

3.2 Ozone loss at high water vapour mixing ratios

For higher water vapour mixing ratios than 12 ppmv, net ozone depletion is simulated (Fig. 3) in the 7-day standard simulation. The ozone loss mechanism generally consists of two steps: a chlorine activation step transferring inactive chlorine (HCl) into active ClO_x followed by catalytic ozone loss processes (Anderson et al., 2012). We analyse both the chlorine activation step and subsequent catalytic ozone loss cycles potentially occurring in mid-latitudes in the lower stratosphere under enhanced water vapour conditions. Since ozone depletion is larger at high water vapour mixing ratios, conditions with a water vapour mixing ratio of 15 ppmv are chosen here to analyse the chemical ozone loss mechanism. Figure 4 shows an overview of the development of important mixing ratios and reaction rates during the 7-day simulation. Panel a illustrates temperature (black line) and surface area density of liquid particles (blue line).

The first phase of the ozone loss mechanism (dark grey background in Fig. 4) is dominated by the occurrence of heterogeneous reactions. The most important heterogeneous chlorine activation reaction is R1 (Fig. 4b), which leads to the chlorine activation chain (von Hobe et al., 2011)

$$\mathrm{ClO} + \mathrm{NO_2} + \mathrm{M} \rightarrow \mathrm{ClONO_2} + \mathrm{M} \quad \text{(R9)}$$

$$\mathrm{ClONO_2} + \mathrm{HCl} \xrightarrow{het.} \mathrm{Cl_2} + \mathrm{HNO_3} \quad \text{(R1)}$$

$$\mathrm{Cl_2} + \mathrm{h}\nu \rightarrow 2\,\mathrm{Cl} \quad \text{(R10)}$$

$$2 \times (\mathrm{Cl} + \mathrm{O_3} \rightarrow \mathrm{ClO} + \mathrm{O_2}) \quad \text{(R11)}$$

net: $\mathrm{HCl} + \mathrm{NO_2} + 2\,\mathrm{O_3} \rightarrow \mathrm{ClO} + \mathrm{HNO_3} + 2\,\mathrm{O_2}$.

This chlorine activation chain yields a transformation of inactive HCl into active ClO_x as well as of NO_x into HNO_3. The ozone loss due to this reaction chain is negligible and no depleting effect on ozone occurs during the first phase (Fig. 4c). In Fig. 4f, the NO_x mixing ratio is seen to decrease and HNO_3 increases due R1. Further, in the first phase the HCl mixing ratio decreases, yielding an increase of ClO_x (Fig. 4f). Both decreasing NO_x and increasing ClO_x have an impact on ozone during the second phase of the ozone loss mechanism (light grey background in Fig. 4), which is characterized by a decreasing ozone mixing ratio (Fig. 4c). The role of NO_x and ClO_x is discussed in detail in the next sections.

3.2.1 Role of NO_x

The transformation of NO_x-radicals into HNO_3 is due to R9 ($ClO+NO_2$) and subsequent the occurrence of the heterogeneous reactions R1 ($ClONO_2 + HCl$) and R2 ($ClONO_2 + H_2O$), which form HNO_3. This behaviour was also found in former studies

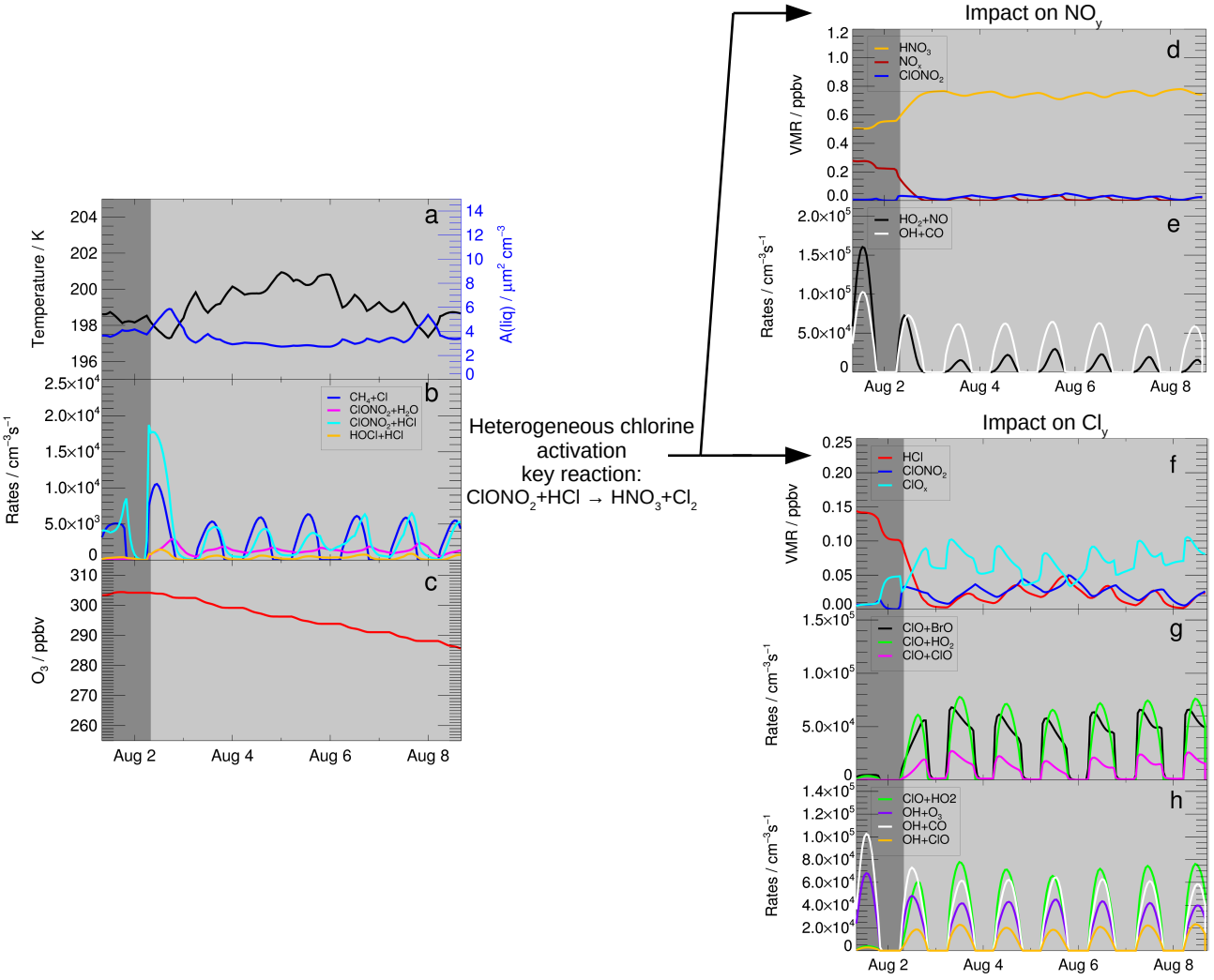

Figure 4. Reaction rates and mixing ratios important for the ozone loss mechanism in the standard simulation using 15 ppmv H_2O. The chlorine activation phase is shaded in dark grey, while the phase of ozone loss has a light grey background. Panel (a) shows the temperature of the trajectory and the liquid surface area density, the ozone mixing ratio is presented in panel (c). Heterogeneous reaction rates are shown in panel (b) as well as the rate of the gas phase reaction $CH_4 + Cl$. Panels (d), mixing ratio of HNO_3 (gas phase + condensed), NO_x and $ClONO_2$, and (e) are relevant to show the role of NO_y for the ozone loss process. Reaction R4 (OH+CO, panel e) limits ozone formation in cycle **C1** at high NO_x mixing ratios and R6 ($HO_2 + NO$) at lower NO_x concentrations. Panels (f)–(h) illustrate the role of chlorine for ozone loss by showing the mixing ratio of HCl, ClO_x and $ClONO_2$ (panel f), main reaction rates (R16 (ClO+ClO), R17 (ClO+BrO), R13 ($ClO + HO_2$)) for catalytic ozone loss cycles (panel g) and potential reaction pathways for the OH-radical (R4 (OH+CO), R18 (OH+ClO), R15 (OH+O_3)) as possible reaction chains following R13 (ClO+HO_2) (panel h). The x-axis ticks refer to 00:00 o'clock local time (06:00 UTC).

(e.g. Keim et al., 1996; Pitari et al., 2016; Berthet et al., 2017), investigating the impact of volcanic aerosols on stratospheric ozone chemistry. Dependent on temperature and water vapour content, the HNO_3 formed remains in the condensed particles. In the standard simulation using 15 ppmv H_2O, 64% of HNO_3 remains in the condensed phase on the day with the lowest temperature (197.3 K, 2 Aug 2013), while at higher temperatures (4–7 August 2013) 85% of HNO_3 are released to the gas phase. After the transformation of NO_x into HNO_3, the NO_x mixing ratio remains low in the second phase of the mechanism (Fig. 4d, light grey region) while the HNO_3 mixing ratio (cond.+gas) remains high.

The transformation of NO_x radicals into HNO_3, due to the occurrence of heterogeneous reactions at elevated water vapour amounts, affects stratospheric ozone chemistry. In the presence of a high NO_x concentration (as at low water vapour mixing ratios), ozone formation in cycle **C1** is determined by the rate of R4 (OH+CO). But if the NO_x concentration is low (as in the second phase of the mechanism), this ozone formation cycle is rate limited by R6 ($NO + HO_2$). For the standard case at 15 ppmv H_2O, both rates are shown in Fig. 4e. In the first phase before NO_x is transferred into HNO_3, cycle **C1** is limited by R4 (OH+CO) which peaks on 1 August 2013 with a maximum rate of $1.0 \cdot 10^5$ cm^{-3}s^{-1}. In the second phase at low NO_x concentrations, cycle **C1** is limited by R6 ($NO + HO_2$) which peaks on 3 August 2013 with a maximum rate of $1.5 \cdot 10^4$ cm^{-3}s^{-1}. Hence, due to the occurrence of the heterogeneous reaction R1 the net ozone formation decreases by at least $3.5 \cdot 10^4$ cm^{-3}s^{-1} from 1 August to 3 August.

3.2.2 Role of ClO_x

In the first phase of the mechanism, chlorine activation yields a transformation of inactive chlorine into active ClO_x. Net chlorine activation occurs when the rates of the heterogeneous reactions R1($ClONO_2 + HCl$), R2 ($ClONO_2 + H_2O$) and R3 (HCl+HOCl) exceed the gas phase HCl formation dominated by the reaction

$$Cl + CH_4 \rightarrow HCl + CH_3. \quad \text{(R12)}$$

Enhanced ClO_x concentrations induce catalytic ozone loss cycles at low temperatures, as the ClO-Dimer-cycle (Molina et al., 1987), the ClO-BrO-cycle (McElroy et al., 1986) and the cycle with ClO and HO_2 (**C2**, Solomon et al., 1986)

$$ClO + HO_2 \rightarrow HOCl + O_2 \quad \text{(R13)}$$

$$HOCl + h\nu \rightarrow Cl + OH \quad \text{(R14)}$$

$$OH + O_3 \rightarrow HO_2 + O_2 \quad \text{(R15)}$$

$$Cl + O_3 \rightarrow ClO + O_2 \quad \text{(R11)}$$

$$\text{net: } 2\,O_3 + h\nu \rightarrow 3\,O_2. \quad \textbf{(C2)}$$

Under conditions of low water vapour (stratospheric background), the rate limiting steps of these cycles are the reactions

$$ClO + ClO + M \rightarrow ClOOCl + M, \quad \text{(R16)}$$

$$ClO + BrO \rightarrow Br + Cl + O_2 \quad \text{(R17)}$$

$$\text{and} \quad ClO + HO_2 \rightarrow HOCl + O_2. \quad \text{(R13)}$$

The rates of the reactions R16, R17 and R13 increase strongly in the second phase of the mechanism (light grey area in Fig. 4g) and thus catalytic ozone loss cycles occur. Under the assumed conditions, ozone depletion is mainly driven by reaction pathways following both R17 and R13. The reaction rates peak on August 3 with a value of $7.8 \cdot 10^4\,\mathrm{cm^{-3}s^{-1}}$ for R13 (ClO+HO_2), $6.8 \cdot 10^4\,\mathrm{cm^{-3}s^{-1}}$ for R17 (ClO+BrO) and $2.7 \cdot 10^4\,\mathrm{cm^{-3}s^{-1}}$ for R16 (ClO+ClO). Additionally the sensitivity of various reaction rates to the water vapour mixing ratio was tested. In Figure 5, the mean reaction rates on 3 August are plotted against the water content assumed during the simulation. Panel (a) shows an acceleration of the ClO-BrO-cycle (based on R17) and **C2** (based on R13) beginning from a water vapour mixing ratio of 11ppmv. The rate determining reaction of the ClO-Dimer-Cycle (R16) increases at a higher water vapour mixing ratio. In contrast, the rate of ozone loss due to the reactions between ClO_x and O_x (O_x=O_3, O) species is negligible here (as shown by the low rate of the reaction $ClO + O(^3P) \rightarrow Cl + O_2$, Fig. 5a).

At stratospheric background conditions with a low water vapour mixing ratio, the rate determining step of cycle **C2** is R13 (Solomon et al., 1986; Ward and Rowley, 2016). For the conditions with enhanced water vapour of 15 ppmv in the standard simulation, the rate of R15 (OH+O_3) is limiting this cycle (Fig. 4f). An investigation of possible reaction pathways of the OH-radical yields that reactions of OH with CO (R4) and ClO (R18) exhibit a rate similar to the reaction with ozone (R15, Fig. 5b).

$$OH + CO \rightarrow H + CO_2 \tag{R4}$$

$$OH + ClO \rightarrow HO_2 + Cl \tag{R18}$$

Based on these reactions, two further reaction chains affecting ozone can be deduced. In cycle **C3**, the OH-radical reacts with CO yielding CO_2 and a hydrogen radical, from which HO_2 is formed. Subsequently HOCl can be formed via R13 (ClO+HO_2) and photolysed in reaction R14. Thus, the net reaction of this pathway is the oxidation of CO to CO_2 and the simultanous destruction of ozone (**C3**).

$$OH + CO \rightarrow H + CO_2 \tag{R4}$$

$$H + O_2 + M \rightarrow HO_2 + M \tag{R5}$$

$$ClO + HO_2 \rightarrow HOCl + O_2 \tag{R13}$$

$$HOCl + h\nu \rightarrow Cl + OH \tag{R14}$$

$$Cl + O_3 \rightarrow ClO + O_2 \tag{R11}$$

$$\text{net: } CO + O_3 + h\nu \rightarrow CO_2 + O_2 \tag{C3}$$

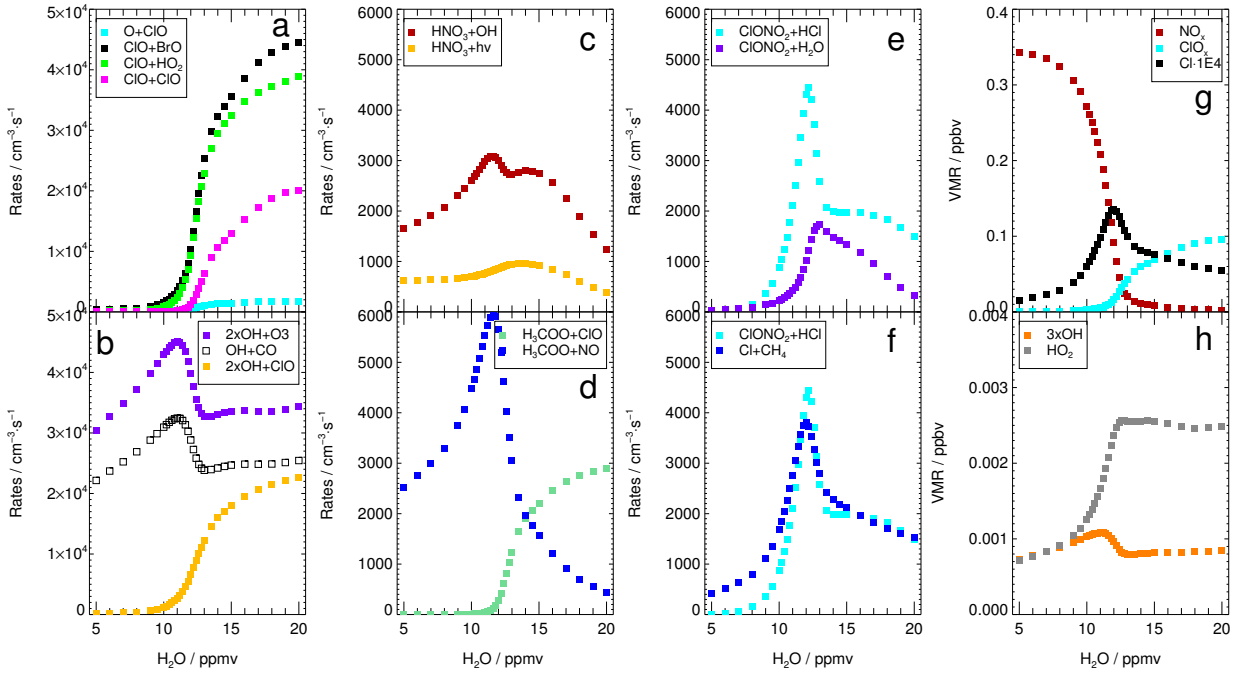

Figure 5. Average reaction rates and volume mixing ratios from the standard simulations on 3rd of August dependent on water vapour content. Panel (a) shows the reaction rates of R16 (ClO+ClO), R17 (ClO+BrO), R13 ($ClO + HO_2$) and $ClO + O(^3P) \rightarrow Cl + O_2$ resulting in ozone reduction, panel (b) possible reaction pathways for the OH radical (R4 (OH+CO), R18 (OH+ClO) and R15 ($OH+O_3$), panel (c) reactions yielding depletion of HNO_3 (R19 ($HNO_3 + OH$), R20 ($HNO_3 + h\nu$), panel (d) reactions of the H_3COO-radical R22 ($H_3COO + ClO$) and R21 ($H_3COO + NO$), panel (e) important heterogeneous reactions (R1 ($ClONO_2 + HCl$), R2 ($ClONO_2 + H_2O$)), and panel (f) the balance between R1 ($ClONO_2 + HCl$) and R12 ($CH_4 + Cl$). Panel (g) shows the mixing ratios of NO_x, ClO_x and 10·Cl and panel (h) the mixing ratios of OH and HO_2.

Furthermore, when the OH-radical reacts with ClO, the products are HO_2 and Cl and thus another catalytic ozone loss cycle **C4** results.

$$OH + ClO \rightarrow HO_2 + Cl \quad \text{(R18)}$$

$$ClO + HO_2 \rightarrow HOCl + O_2 \quad \text{(R13)}$$

$$HOCl + h\nu \rightarrow Cl + OH \quad \text{(R14)}$$

$$2\text{ x } (Cl + O_3 \rightarrow ClO + O_2) \quad \text{(R11)}$$

$$\text{net: } 2O_3 \rightarrow 3O_2 \quad \textbf{(C4)}$$

In the cycles **C2** and **C4** two ozone molecules are destroyed, while one ozone molecule is destroyed in **C3**. To assess the effectiveness regarding ozone loss of **C2** – **C4**, the rate of R4 (limiting **C3**) is compared with two times the rate of R15 (limiting **C2**) and R18 (limiting **C4**). This comparison shows that cycle **C2** is more relevant for ozone loss than **C3** and **C4** (Fig. 5b). However, the relevance of **C4** for catalytic ozone destruction increases for higher water vapour mixing ratios.

A requirement for the effectiveness of the ozone loss cycles is a high mixing ratio of activated chlorine (ClO_x). In Fig. 4b, the rate of the main HCl-foration reaction R12 (Cl+CH_4, dark blue) shows a formation of HCl, which is mainly balanced by the heterogeneous HCl-destruction reaction R1 ($ClONO_2$+HCl) holding the HCl mixing ratio low and thus ClO_x values high. This balance between chlorine activation (R1, $ClONO_2$+HCl) and chlorine deactivation (R12, Cl+CH_4) is schematically illustrated with blue arrows in Fig. 6 and similar to HCl-null-cycles (Müller et al., 2018), which balance gas phase HCl-formation and heterogeneous HCl-destruction under Antarctic polar night conditions. In these polar HCl-null-cycles each HCl formed in reaction R12 is depleted through the heterogeneous reaction R3 (HCl+HOCl). For the conditions in the mid-latitudes during summer considered here, a higher NO_x mixing ratio prevails than under Antarctic ozone hole conditions. As a consequence R1 ($ClONO_2 + HCl$) is here mainly responsible for HCl-depletion. Reaction R1 combined with R9 ($ClO + NO_2$) yields additionally the transformation of NO_x into HNO_3. This HNO_3 formation is balanced by reaction

$$HNO_3 + OH \rightarrow H_2O + NO_3 \qquad \text{(R19)}$$

(see Fig. 6, green), leading to a staedy HNO_3 mixing ratio (Fig. 4d).
A further option to convert HNO_3 into active NO_x may be the HNO_3-photolysis

$$HNO_3 + h\nu \rightarrow NO_2 + OH, \qquad \text{(R20)}$$

but the rate of reaction R19 is more than 2.5 times larger than the rate of the HNO_3 photolysis (R20, Fig. 5c). Hence, the heterogeneous reaction R1 couples two pathways: A pathway balancing HCl-destruction in R1 and HCl-formation in R12 ($Cl + CH_4$) and thus maintaining a high ClO_x mixing ratio, and a pathway balancing HNO_3-formation in R1 and HNO_3 destruction in R19 and thus maintaining a low NO_x mixing ratio.

The balance of radical species, which are converted in both pathways, additionally links both pathways (Fig. 6, light colours). In reaction R12, besides HCl a methylperoxy radical (H_3COO) is formed, which reacts either with NO or with ClO leading to HO_x-formation (HO_x=H, OH, HO_2).

$$H_3COO + NO \rightarrow HCHO + H + NO_2 \qquad \text{(R21)}$$

$$H_3COO + ClO \rightarrow HCHO + HO_2 + Cl \qquad \text{(R22)}$$

In reaction R19, HNO_3 is depleted in a reaction with an HO_x-radical (Fig. 6, yellow). How the H_3COO-radical reacts, depends on the mixing ratios of ClO_x and NO_x. For water vapour mixing ratios around the water vapour threshold, the NO_x mixing ratio is higher than the ClO_x mixing ratio (Fig. 5g). Hence, the methylperoxy radical rather reacts with NO than with ClO (Fig. 5d) leading to pathway (a) in Fig. 6. At higher water vapour mixing ratios, H_3COO rather reacts with ClO (R22) leading

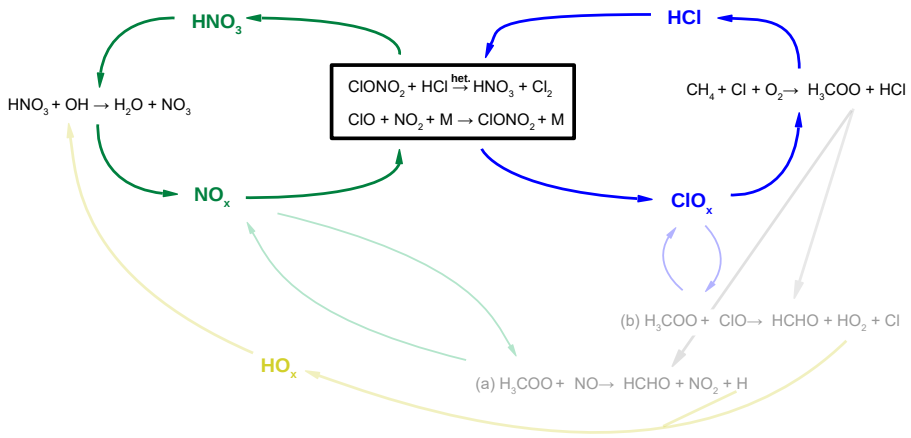

Figure 6. Reaction scheme to illustrate the balance between chlorine activation and chlorine deactivation (blue, right) and NO_x activation and deactivation (green, left). The heterogeneous reaction $ClONO_2$+HCl (R1) links both cycles. Additional reaction pathways, which balance radicals are shown in light colours.

to pathway (b) in Fig. 6. The balance between HCl-formation and -destruction as well as HNO_3-formation and -destruction due to the occurrence of the heterogeneous reaction R1 is analysed in detail in the Appendix A.

In this example the heterogeneous HCl-destruction (R1, $ClONO_2$+HCl) does not balance the HCl-formation (R12, $Cl + CH_4$) (Fig. 4b) completely, because of increasing temperatures (Fig. 4a). Higher temperatures decelerate the heterogeneous HCl-destruction and thus result in the slightly increasing HCl-mixing ratio from 4 August–7 August 2013 (Fig. 4f). Such temperature fluctuations (Fig. 4a) affect the balance between HCl formation and destruction less at higher water vapour mixing ratios, because the heterogeneous HCl-destruction rate (R1) increases for both low temperatures and high water vapour mixing ratios (see Sec. 4). Thus, regarding the balance between HCl formation and HCl destruction (and hence the balance between chlorine deactivation and chlorine activation), a high water vapour mixing ratio can compensate a small range of temperature fluctuations. This balance maintains activated chlorine levels, which is essential for catalytic ozone loss cycles to proceed.

4 Analysis of chlorine activation

In the previous section we showed that in the temperature range of 197–202 K there is a threshold for water vapour, which has to be exceeded to yield chlorine activation and thus enables substantial ozone destruction. Here, we investigate the sensitivity of this threshold on sulphate content, temperature, Cl_y and NO_y mixing ratio.

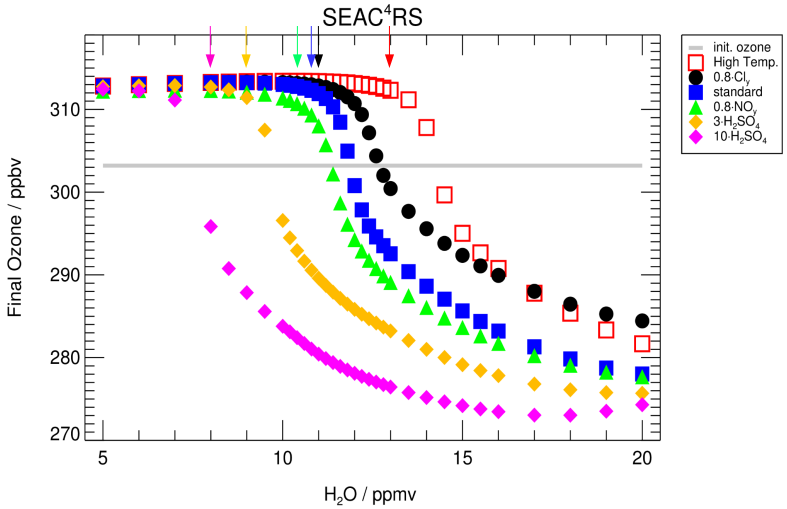

Figure 7. Impact of the water vapour content on the ozone mixing ratio (final ozone) reached at the end of the 7-day simulation along the standard trajectory (SEAC^{4}RS). The standard case is shown in blue and the initial ozone amount is marked by the grey line. An impact on the final ozone mixing ratios is observable after exceeding a critical threshold in water vapour, which is marked with an arrow for the different cases. This threshold changes with a shift in trajectory temperature (+1K, red), the Cl_y mixing ratio to 0.8 Cl_y (black), the NO_y mixing ratio (0.8 NO_y, green) and the sulphate content (3× standard H_2SO_4, yellow and 10× standard H_2SO_4, magenta).

4.1 Sensitivity of the water vapour threshold

Modifying temperature, sulphate amount or the mixing ratios of Cl_y or NO_y yields a shift of the water vapour threshold. Figure 7 shows the ozone values reached at the end of the 7-day simulation (final ozone) for a variety of sensitivity cases assuming the standard trajectory. For each case, the water vapour threshold is marked with an arrow in the colour of the corresponding case.

The water vapour dependent final ozone values for the standard case are plotted as blue squares (Fig. 7) with a water vapour threshold of 10.6 ppmv (see Sec. 3). Raising the trajectory temperature by 1 K over the standard case leads to a higher water vapour threshold of 13.0 ppmv (open red squares), while increasing the sulphate content by a factor of 3 results in a lower threshold region of ∼9.0 ppmv (yellow diamonds). An even larger enhancement of the sulphate content (10× H_2SO_4, magenta diamonds) lowers the water vapour threshold further to a value near ∼8 ppmv. Reducing the NO_y mixing ratio to 80% of the standard case yields a shift of the threshold to a lower water vapour mixing ratio (green filled triangles), while an equivalent reduction in the Cl_y mixing ratio shifts the threshold to higher water vapour mixing ratios (black circles). A reduction in Cl_y also reduces ozone destruction and hence results in higher ozone mixing ratios at the end of the simulation. The sensitivity of

the water vapour threshold to temperature, sulphate abundance and Cl_y and NO_y mixing ratio is explained in the next Section (Sec. 4.2).

As a further example for an event with high stratospheric water vapour mixing ratios based on airborne measurements, simulations based on measurements during the Mid-latitude Airborne Cirrus Properties Experiments (MACPEX) were conducted. This campaign was based in Texas during springtime 2011 and hence prior to the formation of the North American Monsoon (NAM). A detailed description of this MACPEX case is given in the Appendix (App. B). For the MACPEX case, changes in sulphate, Cl_y and NO_y mixing ratios affect the water vapour threshold similarly to that observed for the SEAC^{4}RS trajectory. Thus, the MACPEX results confirm the SEC^{4}RS findings. Therefore, we conclude that in the considered temperature range ($\sim$197–202 K), an ozone reduction occurs after exceeding a water vapour threshold and that this threshold varies with Cl_y, NO_y, sulphate content and temperature.

4.2 Explanation of the water vapour threshold

The sensitivity of the water vapour threshold to Cl_y, NO_y, sulphate loading and temperature is investigated, focussing on the balance between heterogeneous chlorine activation mainly due to R1 ($ClONO_2 + HCl$) and gas phase chlorine deactivation mainly due to R12 ($Cl + CH_4$). Net chlorine activation takes place when the chlorine activation rate exceeds the chlorine deactivation rate. Reaction R1 is the key reaction in the chlorine activation process. Therefore, in the following, first the dependence of R1 on the water vapour content is analysed in detail. Second, the balance between chlorine activation and deactivation is investigated, also considering the impact of Cl_y, NO_y, sulphate and temperature on the water vapour threshold. In general the rate of R1 ($ClONO_2 + HCl$) v_{R1} is determined through:

$$v_{R1} = k_{R1} \cdot c_{ClONO_2} \cdot c_{HCl} \tag{R23}$$

The concentrations of $ClONO_2$ c_{ClONO_2} and HCl c_{HCl} are associated with the gas phase mixing ratio and the rate constant k_{R1}, as a measure of the reactivity of the heterogeneous reaction, depends in this case on the γ-value γ_{R1}, the surface area of the liquid particle A_{liq}, the temperature T and c_{HCl} (Eq. R24) (Shi et al., 2001).

$$k_{R1} \propto \frac{\gamma_{R1} \cdot A_{liq} \cdot \sqrt{T}}{1 + c_{HCl}} \tag{R24}$$

The γ-value describes the uptake of $ClONO_2$ into liquid particles due to the decomposition of $ClONO_2$ during reaction R1 and is thus a measure of the probability of the occurrence of this heterogeneous reaction (Shi et al., 2001). Laboratory studies showed a dependence of γ_{R1} on the solubility of HCl in the droplet, which generally increases for a lower H_2SO_4 fraction in the particle (H_2SO_4 wt%) (Elrod et al., 1995; Hanson, 1998; Zhang et al., 1994; Hanson and Ravishankara, 1994). From Eq. R24 it is obvious that a large surface area A_{liq} and a high γ-value γ_{R1} increase k_{R1} and thus the heterogeneous reaction rate v_{R1}.

In Figure 8, the impact of the water vapour content on the H_2SO_4 weight-percent, γ_{R1}, A_{liq}, k_{R1} and the reaction rate v_{R1} is shown. To avoid the influence of R1 itself on these parameters as much as possible, these parameters are selected for 1 August 2013 at 13:00 UTC. This point in time corresponds to the values after the first chemistry time step during the chemical simulation. The particles H_2SO_4 wt% decreases for all cases with increasing water vapour from more than 50 wt% at 5 ppmv

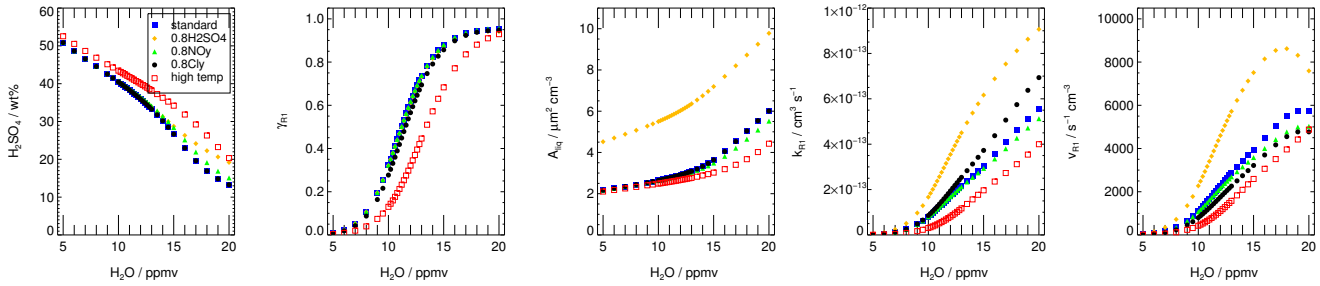

Figure 8. Dependence on water vapour of the rate of the the main heterogeneous chlorine activation reaction R1 v_{R1}, the rate coefficient (k_{R1}), the γ-value γ_{R1}, the liquid surface area density A_{liq}, and the H_2SO_4 weight %. Presented parameters correspond to the values after the first chemistry time step of the box-model simulation. Additionally the impact of an enhanced sulphate content (0.8 ppbv H_2SO_4, yellow), reduced NO_y (0.8 NO_y, green), reduced Cl_y (0.8 Cl_y, black) and enhanced temperatures (red) is shown. The standard case is shown as blue squares.

H_2O to around 20 wt% at 20 ppmv H_2O due to an inceasing uptake of H_2O in the thermodynamic equilibrium. The standard case is illustrated in blue squares (Fig.8) and exhibits a strongly increasing gamma value especially for water vapour mixing ratios between 9 and 14 ppmv due to a lower H_2SO_4 wt%. In the same water vapour range, the liquid surface area density A_{liq} increases slightly. It increases more for higher water vapour mixing ratios because of HNO_3 uptake into the particles. Due to the increasing γ-value with increasing water vapour, the rate constant k_{R1} increases (Shi et al., 2001) and thus induces a larger reaction rate v_{R1} with an increasing water vapour mixing ratio.

At low water vapour mixing ratios, not only the rate of R1 ($ClONO_2 + HCl$) but also of R12 ($CH_4 + Cl$) increases with an

increasing water content (Fig. 5f). An increasing heterogeneous reaction rate (R1) results in both a lower NO_x mixing ratio and more HCl converted into ClO_x. A higher ClO_x concentration yields a higher Cl mixing ratio and thus an increase in the rate of R12 ($CH_4 + Cl$). Since both the rates of R1 and R12 increase, no significant net chlorine activation occurs. Around the water vapour threshold, the Cl-mixing ratio peaks (Fig. 5g), because less ClO is converted into Cl through

$$ClO + NO \rightarrow Cl + NO_2 \tag{R25}$$

due to the decreasing NO_x mixing ratio. The lower Cl mixing ratio reduces the HCl formation in R12 ($CH_4 + Cl$). Hence, the increasing heterogeneous reactivity k_{R1} yields a higher rate of R1 and in the same way it impedes R12 by reducing the NO_x mixing ratio. As a consequence the rate of R1 exceeds the rate of R12 and a net chlorine activation takes place, leading to a reduction of HCl. The decline in both HCl and NO_x yields smaller rates of R1 and R12 at high water amounts and thus a peak of R1 and R12 (Fig. 5f). Hence, the increasing heterogeneous reactivity (k_{R1}) of R1 destabilizes the balance between chlorine activation and deactivation by promoting the chlorine activation (due to an increasing rate of R1) and impeding chlorine deactivation (due to a reduction of R12). This yields heterogeneous chlorine activation to exceed gas phase HCl-formation in the water vapour threshold region.

For an enhanced sulphate content (Fig. 8, yellow diamonds), the particle surface area density (A_{liq}) is larger, leading to both a stronger increase of the heterogeneous reactivity (k_{R1}) and hence a higher heterogeneous reaction rate than in the standard case. Due to this higher heterogeneous reactivity (k_{R1}), the chlorine activation rate exceeds the chlorine deactivation at a lower water vapour mixing ratio and the net chlorine activation is reached at a lower water vapour threshold. A shift to higher temperatures (Fig. 8, red) yields almost no change in the surface area density (A_{liq}) but a reduced γ-value due to a higher H_2SO_4 fraction in the particles (H_2SO_4 wt%) and thus a lower heterogeneous reactivity (k_{R1}). The reduced reactivity causes the net chlorine activation to occur at a higher water vapour threshold.

In contrast, the shift of the threshold for simulations with only 80% of standard NO_y (0.8 NO_y, Fig. 8 green) or Cl_y (0.8 Cl_y, Fig. 8 black) can not be explained only by an increase in k_{R1}. In these cases, further effects on the balance between chlorine activation and chlorine deactivation have to be taken into account. The water vapour threshold in the 0.8 NO_y simulation (green triangles) is shifted to lower water vapour values due to a smaller Cl/ClO-ratio for lower NO_x concentrations. This yields a reduced HCl formation through R12 ($CH_4 + Cl$) than in the standard case and thus impedes chlorine deactivation. The reduced chlorine deactivation affects the balance between chlorine activation and deactivation in a way that the water vapour threshold region in the 0.8 NO_y case is lower than in the standard case. In the 0.8 Cl_y case (Fig. 8, black), the HCl and $ClONO_2$ mixing ratios are reduced. This leads to a lower chlorine activation rate v_{R1} than in the standard case, despite of the slight higher heterogeneous reactivity (k_{R1}), which is due to the inverse dependence of k_{R1} on the HCl concentration (Eq. R24). The lower dependence of reaction R12 (Cl+CH_4) than of R1 ($HCl + ClONO_2$) on the Cl_y mixing ratio would push chlorine deactivation (R12) in the balance between chlorine activation and deactivation and hence shift the water vapour threshold to higher water vapour mixing ratios. Additionally caused by the lower rate of R1 ($ClONO_2 + HCl$) for reduced Cl_y, the NO_x mixing ratio decreases more slowly. This enhances the rate of R12 compared with the standard case as well, because more NO_x yields a higher Cl/ClO-ratio.

In summary, the water vapour threshold is determined by the balance between chlorine activation and deactivation and is thus in a certain temperature range especially sensitive to the water dependence of the heterogeneous reactivity (k_{R1}) mainly described through the γ-value γ_{R1} and the particle surface A_{liq}. These parameters are dependent on the present temperature and sulphate content. However, further parameters influencing this balance, such as the NO_y and Cl_y mixing ratio, have an impact on the water vapour threshold as well.

4.3 Temperature dependence

The water vapour threshold, which has to be exceeded for chlorine activation and stratospheric ozone loss to occur, is mainly dependent on the temperature. To illustrate the impact of both temperature and water vapour mixing ratio on stratospheric ozone, the relative ozone change occurring after a 7-day simulation, in which a constant temperature and water vapour concentration and the Cl_y and NO_y values of the standard case are assumed, is shown in Fig. 9. In the left panel, ozone change as a function of temperature and water vapour is plotted for non-enhanced sulphate amounts. In the right panel, the relative ozone change is shown for 10× standard sulphate to estimate a potential impact of volcanic eruptions or sulphate geoengineering on stratospheric ozone. Since mixing of neighbouring air parcels is neglected in the box-model study, the relative ozone change calculated corresponds to the largest possible ozone change for the conditions assumed. A mixing of moist tropospheric air with dry stratospheric air is expected to reduce the water vapour mixing ratio during the time period of the 7-day trajectory and hence could stop ozone depletion before the end of the trajectory is reached. In addition to the relative ozone change, the threshold for chlorine activation is shown as a white line in both panels. When temperature is held constant, this threshold corresponds to the water vapour threshold discussed above. Chlorine activation occurs at higher water mixing ratios and lower temperatures relative to the white line plotted. Here, chlorine is defined to be activated, if the ClO_x/Cl_y ratio exceeds 10%.

For climatological non-enhanced sulphate amounts (Fig. 9, left), the temperature has to fall below 203 K for chlorine activation to occur, even for high water vapour mixing ratios of 20 ppmv. For the simultaneous presence of high water vapour and low temperatures an ozone loss of 9% (max. 27 ppbv O_3) was found. This maximal ozone loss occurs for a range of low temperatures (195–200 K) and enhanced water vapour mixing ratios (10–20 ppmv), because of a similar time until chlorine activation occurs. If the temperatures are higher and water vapour mixing ratios lower than the chlorine activation line, the ozone mixing ratio increases around 3.5% ($\sim$ 10 ppbv O_3). At enhanced sulphate conditions (Fig. 9, right) an ozone loss of max. 10% (30 ppmv O_3) occurs for low temperatures and high water vapour mixing ratios. For a water vapour mixing ratio of 20 ppmv the temperature has to fall below 205 K for ozone loss to occur. If the temperatures are very low (195–200 K) and the water vapour is high (10–20 ppmv) ozone loss is slightly reduced. This turnaround occurs, because at a high sulphate loading in combination with high water and low temperatures more HCl is taken up by condensed particles. This leads to less Cl_y in the gas phase and thus lower rates of catalytic ozone loss.

In summary, the combination of low temperatures, enhanced sulphate concentrations and high water vapour mixing ratios promotes an ozone decrease of up to $\sim$10% (corresponding to maximum -30 ppbv O_3). In comparison to the study of Anderson et al. (2012), the temperatures have to fall below 203 K (here) instead of 205 K (in Anderson et al. (2012)) for non enhanced sulphate conditions and below 205 K instead of 208 K (in Anderson et al. (2012)) for enhanced sulphate conditions and a water

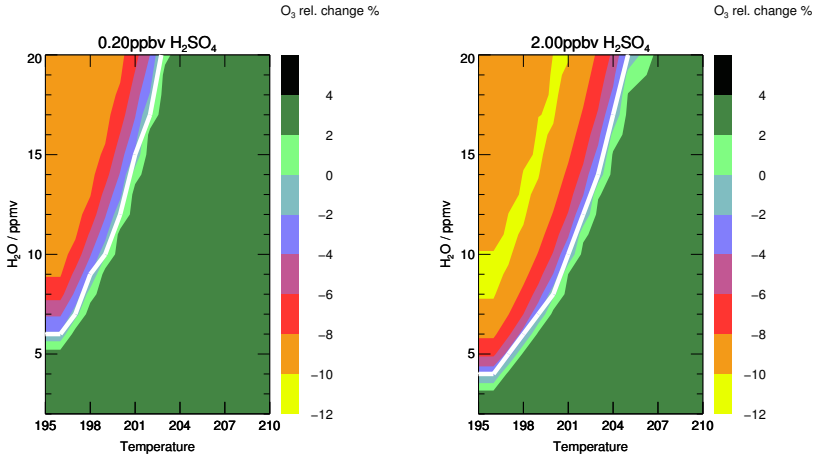

Figure 9. Relative ozone change during the 7-day simulation along the standard trajectory dependent on temperature and H_2O ratio for climatological non enhanced (left panel) and enhanced (right panel) sulphate conditions. The white line corresponds to the water and temperature dependent chlorine activation threshold.

vapour mixing ratio of 20 ppmv for chlorine activation and thus ozone loss to occur. Hence, Anderson et al. (2012) found ozone loss in mid-latitudes at high water vapour mixing ratios for temperatures 2 to 3 K higher than in our simulations.

5 Case studies

Case studies were conducted to illustrate the sensitivities described above on ozone loss and to estimate the impact of realistic conditions and an upper boundary on the ozone loss process. In the "case based on observations", standard conditions and the measured water vapour mixing ratio of 10.6 ppmv were assumed using both the low sulphate content of the standard case and a slightly enhanced sulphate content, which represents the possible impact of volcanic eruptions or geoengineering conditions. As a kind of worst case study (upper boundary), the "Case of high Cl_y" was simulated using Cl_y and NO_y mixing ratios based on the study of Anderson et al. (2012), which uses Cl_y and NO_y much larger than inferred from tracer-tracer correlations (Table 1). In the "reduced Br_y case", standard conditions with a 50% reduced Br_y mixing ratio were assumed to test uncertainties in current observations of stratospheric bromine burden. Additionally the previously noted standard 7-day trajectory was extended to a 19-day trajectory to infer the dependence of ozone loss on the simulated time period.

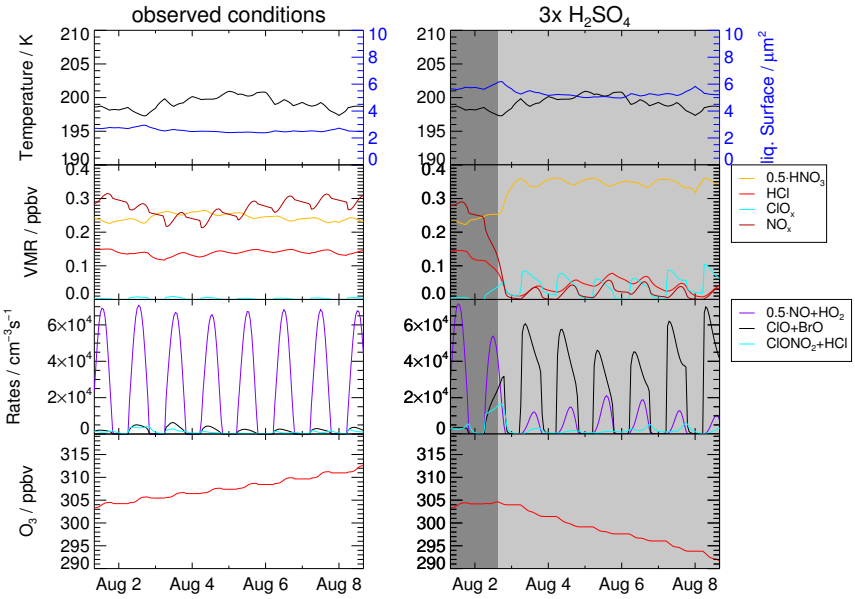

Figure 10. Left panels present the temperature, liquid surface area density, ozone mixing ratio, reaction rates of R1 ($ClONO_2 + HCl$, cyan), R17 (ClO+BrO, black) (as an example for ozone loss cycles), R6 ($NO + HO_2$, violet) which limits ozone formation at low NO_x concentrations as well as volume mixing ratios of HCl (red), ClO_x (light blue), NO_x (black) and HNO_3 (scaled with 0.5) for the "Case based on observations" with 10.6 ppmv H_2O and 0.20 ppbv H_2SO_4. The panels on the right show the same quantities, but for enhanced sulphate conditions (0.60 ppbv H_2SO_4). The x-axis ticks refer to 00:00 local time (06:00 UTC) of that day.

5.1 Case based on observations

The simulation of the case based on observations during the SEAC^{4}RS aircraft campaign corresponds to the most realistic case for today's chemical conditions. It is identical to that of the standard case but assumes a fixed water vapour mixing ratio of 10.6 ppmv observed on 8 August 2013. Under these conditions, neither relevant heterogeneous chlorine activation due to R1 ($ClONO_2 + HCl$) nor catalytic ozone loss cycles (e.g. based on ClO+BrO) can be observed in the simulation (Fig. 10, left). Instead, ozone is formed. In comparison, the same simulation with 0.6 ppbv gas phase equivalent H_2SO_4 instead of 0.2 ppbv was conducted (Fig. 10, right). The enhanced sulphate content yields a larger liquid surface area density and thus an increased heterogeneous reactivity. Hence, reaction R1 occurs in the $3\times H_2SO_4$ simulation significantly, leading to a slightly increasing ClO_x mixing ratio and a decrease of the NO_x mixing ratio. Both a reduced ozone formation in **C1** (which is at decreased NO_x concentrations limited by R6) and ozone loss cycles (e.g. based on the reaction ClO+BrO or $ClO+HO_2$) can be observed, resulting in a reduction of ozone.

Using initial conditions, the trajectory corresponding to the SEAC^{4}RS observations shows ozone loss with sulphate enhanced by a factor of 3. However, we note that this was an unusually cold trajectory. A more common case with higher mean temperatures would require a higher sulphate content to enhance the heterogeneous reactivity that chlorine activation can occur. Thus

under current chemical conditions in the UTLS (upper troposphere, lower stratosphere), it is most unlikely to get significant ozone loss by convectively injected water vapour in mid-latitudes.

5.2 Case of high Cl_y

Under conditions of substantially higher initial Cl_y and NO_y mixing ratios (see Tab. 1) than in the standard case used in Anderson et al. (2012), a larger ozone loss up to 265 ppbv during the 7-day simulation is simulated (Fig. 11a). Since these high Cl_y conditions have been criticised in other studies (e.g. Schwartz et al., 2013; Homeyer et al., 2014) as being unrealistically high, they are assumed here as a worst case scenario. Under high chlorine conditions, and for a high water vapour content (more than ≈18 ppmv), an almost complete ozone destruction with a final ozone value of less than 50 ppbv is simulated (Fig. 11a), which corresponds to parcel ozone loss of 85%. During the 3.5-day simulation in the study of Anderson et al. (2012), an ozone loss of 20% with respect to initial ozone occurs for 18 ppmv H_2O. This difference in relative ozone loss for similar conditions here and in the study of Anderson et al. (2012) is caused by a longer assumed ozone destruction period in our simulation. Since the Cl_y-mixing ratio is much higher than in the standard case, the catalytic ozone loss cycles are dominated by the ClO-Dimer cycle (see S1 in the Supplements for chemical details). Assuming the measured water vapour content of 10.6 ppmv for high chlorine conditions would lead to an ozone depletion of 57% during the 7-day simulation. In comparison, in the standard case an ozone loss of 8% is reached when a high water vapour mixing ratio of 20 ppmv is assumed. However, even for the standard trajectory and a high chlorine content, a water vapour amount of 8 ppmv has to be exceeded to yield any ozone reduction. This threshold shifts from 8 ppmv to 7 ppmv for the case where stratospheric sulphate is tripled (Fig. 11a, yellow triangles).

5.3 Reduced Br_y Case

The mixing ratio of inorganic bromine (Br_y) has a high uncertainty in the lowermost stratosphere due to the influence of very short lived bromine containing substances. For example, during the CONTRAST field campaign (Jan-Feb 2014, western Pacific region), Koenig et al. (2017) observed a Br_y mixing ratio in the lower stratosphere of 5.6–7.3 pptv and the contribution of Br_y, which crosses the tropopause, was estimated to be 2.1±2.1 pptv (Wales et al., 2018). Navarro et al. (2017) found somewhat different bromine partitioning depending on the ozone, NO_2 and Cl_y concentrations, using very short lived bromine species observations in the eastern and western Pacific ocean from the ATTREX campaign. Because our Br_y values are not based on measurements for this specific case modelled, we tested the sensitivity to a value that is half of our standard case. The impact of this Br_y reduction is illustrated in Fig. 11b.

Comparing the final ozone value for the 0.5 Br_y simulations (Fig. 11b, light blue triangles) with those of the standard case (blue squares), a higher water vapour threshold and a reduced ozone loss of about 30% at high water vapour mixing ratios is simulated. The shift of the water vapour threshold is due to the impact of Br_y on the NO_2/NO-ratio. Due to the reaction

$$BrO + NO \rightarrow Br + NO_2, \tag{R26}$$

reduced Br_y yields a smaller NO_2/NO-ratio and hence less $ClONO_2$ formation in R9 (ClO+NO_2). Since $ClONO_2$ formation is essential for chlorine activation in R1 ($ClONO_2$+HCl), reduced Br_y yields a lower chlorine activation rate (von Hobe et al.,

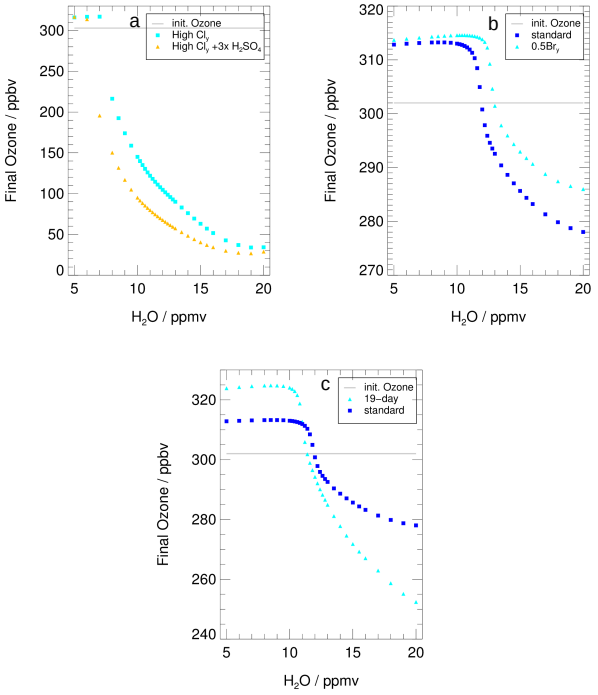

Figure 11. The water dependent final ozone value is shown for (a) the "Case of high Cl_y" (see Tab. 1 for NO_y and Cl_y initialisation) assuming background aerosol (light blue) and tripled H_2SO_4 (yellow), (b) reduced Br_y (light blue, "Reduced Br_y case"), and (c) an extended time period of activated chlorine (light blue, "19-day simulation"). In panel (b) and (c) also final ozone of the standard case is shown (blue). Initial ozone is marked with a grey line. Note that the scale of all y-axis differ.

2011) and thus a shift of the water vapour threshold to higher water vapour mixing ratios. In the case of reduced Br_y, less ozone is destroyed regarding the standard case. The ozone destruction in the ClO-BrO-cycle is reduced, while the rates of R16 (ClO+ClO) and R13 (ClO+HO_2) are similar to those of the standard case (Fig. 4,e; for chemical details of the reduced Br_y-case see Suppl. S2). This results in the reduced ozone destruction in the 0.5 Br_y case.

5.4 Extended time period

Since the occurrence of the ozone loss process analysed in this study is strongly dependent on a variety of parameters, the time period over which the ozone loss might occur is very uncertain. The impact of this time period on ozone loss was tested by extending the 7-day trajectory used in the sections above to span the entire period with temperatures low enough to maintain chlorine activation. In this time extended simulation, temperatures are well below 200 K at the begin of the simulation and remain below 201 K for 14 days. Hence, chlorine activation can be maintained for a longer time period than in the standard case and breaks up due to increasing temperatures (for details regarding chemical processes and temperature development

along the extended trajectory see Suppl. S3).

Because of the extended time period, the final ozone values using the enhanced water vapour mixing ratios for the longer trajectory (cyan triangles Fig. 11c) are much lower than those of the standard 7-day simulation (blue squares). Additionally, more ozone is formed when using low water vapour concentrations. Comparing the water vapour threshold of the 7-day trajectory ($\sim$10.6 ppmv) and the 19-day simulation (10.2 ppmv), a shift to lower water vapour mixing ratios occurs in the 19-day trajectory. This shift is likely due to an extended time period with a temperature well below 200 K at the begin of this trajectory, which allows a chlorine activation to occur even for slightly lower water vapour amounts. Simulations along a trajectory starting on the same day as the 7-day trajectory, but finishing on 15 August, yield the same water vapour threshold as the 7-day simulation (not shown), indicating that the shift in the threshold shown in Fig. 11 is associated with the very cold conditions at the start of the 19-day simulation. Hence, the length of the chosen trajectory has no impact on the water vapour threshold, but does effect the final ozone.

6 Discussion

Many uncertainties affect the assessment of the extent of ozone loss that occurs in the lowermost stratosphere at mid-latitudes under enhanced water vapour conditions. The number and depth of convective overshooting events as well as the area and duration affected by enhanced water vapour mixing ratios is a subject of recent research (e.g. Homeyer et al., 2014; Smith et al., 2017). The mixing ratios of important trace gases (O_3, Cl_y, Br_y, NO_y) in overshooting plumes and the probability that water vapour mixing ratios high enough for chlorine activation meet temperatures low enough is a matter of debate (e.g. Schwartz et al., 2013; Homeyer et al., 2014).

The ozone loss mechanism investigated here requires the occurrence of the heterogeneous reaction R1, which leads to enhanced ClO_x and reduced NO_x mixing ratios and thus maintains effective catalytic ozone loss cycles. Enhanced ClO and reduced NO concentrations were observed by Keim et al. (1996) and Thornton et al. (2007) close to the mid-latitude tropopause under conditions with both enhanced water vapour and enhanced concentrations of condensation nuclei, such as sulphate particles. These observations were attributed to the occurrence of the heterogeneous reactions R1 ($ClONO_2$+HCl) and R2 ($ClONO_2 + H_2O$, Thornton et al., 2007; Keim et al., 1996). For the temperature and the water vapour range observed in the studies of Keim et al. (1996) (15 ppmv H_2O, $\sim$207 K) and Thornton et al. (2007) (15–22 ppmv H_2O, $\sim$213–215 K), a heterogeneous chlorine activation would not occur in the box-model simulation conducted here, not even in a sensitivity simulation assuming a high sulphate gas phase equivalent of 7.5 ppbv H_2SO_4 (not shown). At low temperatures ($\lesssim$196 K), heterogeneous chlorine activation may occur in the tropical stratosphere (Solomon et al., 2016; von Hobe et al., 2011). Von Hobe et al. (2011) observed enhanced ClO mixing ratios during aircraft campaigns over Australia (SCOUT-O_3, 2005) and Brazil (TROCCINOX, 2005) in combination with low temperatures and the occurrence of cirrus clouds. Analysing the balance between chlorine activation and deactivation von Hobe et al. (2011) showed an increase of the chlorine activation rate (R1) with a higher ClO, BrO and O_3 mixing ratio. Thus, once started, R1 accelerates due to higher ClO-mixing ratios subsequently yielding a fast conversion of NO_x into HNO_3 (von Hobe et al., 2011), comparable to the NO_y repartitioning found in the present study. Von Hobe et al.

(2011) found a threshold in ozone mixing ratio, which has to be exceeded for chlorine activation to occur. Hence, the water vapour threshold discussed here is expected to depend on the ozone mixing ratio, as well. Furthermore a potential occurrence of ice particles in the lowermost mid-latitude stratosphere (Spang et al., 2015) might affect the water vapour threshold due to a different heterogeneous reactivity on ice than on liquid particles (Solomon, 1999).

An enhanced sulphate content increases the heterogeneous reaction rate caused by an enlarged liquid surface. Due to this relation, an impact of stratospheric albedo modification (by applying solar geoengineering) on the ozone loss process proposed by Anderson et al. (2012) is discussed (Dykema et al., 2014). Applying solar geoengineering would also affect the temperature in the lowermost stratosphere by perturbing the Eddy-heat fluxes and would change the lower stratospheric dynamics (Visioni et al., 2017). It would also affect large scale latitudinal mixing of atmospheric tracers in the lower branch of the Brewer-Dobson-Circulation leading to a different level of isolation of the tropical pipe with mid-latitudes and would result in a different chemical composition of the lower mid-latitude stratosphere (Visioni et al., 2017). Varying the sulphate content in our study showed that for temperatures and water vapour conditions of the case based on observations, a moderate enhancement of $3\times H_2SO_4$ is sufficient to yield ozone depletion. Considering the temperature and water vapour dependence of the chlorine activation line (Fig. 9, white line), a $10\times$ enhancement of stratospheric sulphate yields a shift of chlorine activation to slightly lower water vapour mixing ratios and higher temperatures. However, even for enhanced sulphate and a water vapour mixing ratio of 20 ppmv, the temperature has to fall below 205 K for chlorine activation (and hence ozone depletion) to occur at the assumed Cl_y and NO_y conditions of the standard case.

After the chlorine activation step, catalytic ozone loss cycles can occur: the ClO-Dimer cycle, the ClO-BrO-cycle and cycles subsequent to R13 ($ClO + HO_2$, **C2**–**C4**). Cycle **C2** is reported to have an impact on stratospheric ozone in mid-latitudes in previous studies (e.g. Johnson et al., 1995; Kovalenko et al., 2007; Ward and Rowley, 2016). Here, **C2** was found to be the dominate cycle based on R13 under standard conditions. Nevertheless, simulating the "0.5 Br_y" and "high Cl_y" case has shown that the relevance of the ClO-Dimer-cycle and the ClO-BrO-cycle depends on the assumed initial values of Cl_y and Br_y. Anderson and Clapp (2018) discussed the occurrence of the ClO-Dimer cycle and the ClO-BrO-cycle dependent on water vapour, the Cl_y mixing ratio and temperature. They illustrate a significant increase in the rate of R16 (ClO+ClO) and R17 (ClO+BrO) if the combination of enhanced water vapour and low temperatures is sufficient for chlorine activation to occur. If chlorine activation occurs in their model study, a higher Cl_y mixing ratio yields higher catalytic ozone loss rates (R16, R17). Their finding regarding the effect of temperature, water vapour and chlorine on the ozone loss process is consistent with the results found here. The occurrence of net chlorine activation is determined by temperature and water vapour mixing ratio, while the Cl_y mixing ratio controls how much ozone is destroyed.

A measure for the effect of temperature and water vapour on stratospheric chlorine activation and ozone chemistry is the temperature and water vapour dependent chlorine activation line (Fig. 9, white line). Anderson et al. (2012) reported that lower temperatures than 205 K are necessary for chlorine activation to occur at a water vapour mixing ratio of 20 ppmv and a climatological non enhanced sulphate content. In comparison, assuming standard conditions for Cl_y and NO_y but a constant temperature here, temperatures lower than 203 K are required for ozone loss to occur at similar H_2O and sulphate concentrations. The standard trajectory was chosen here to hold for conditions most likely for chlorine activation based on SEAC^{4}RS

measurements.For the temperature range of this trajectory and the measured water vapour mixing ratio (10.6 ppmv) no significant ozone depletion occurs. Hence, for all SEAC^{4}RS and MACPEX trajectories calculated (not only the shown examples), no trajectory produced ozone loss. A further requirement for the occurrence of chlorine activation is the maintenance of the conditions, which yield chlorine activation, during the entire time of chlorine activation. Assuming standard conditions and a water vapour mixing ratio of 20 ppmv, chlorine activation takes 5 hours. However for a water vapour content close to the water vapour threshold, low temperatures and enhanced water vapour mixing ratios have to be maintained 24–36 hours for chlorine activation to have an impact on stratospheric ozone chemistry. For the occurrence of ozone depletion, temperatures have also to remain low and water vapour mixing ratios high after the chlorine activation step.

The maximum ozone depletion at standard conditions occurs here for a water vapour mixing ratio of 20 ppmv. Final ozone assuming 20 ppmv H_2O in the 7-day simulation is 11% lower than the final ozone reached under atmospheric background conditions assuming 5 ppmv H_2O. For the 19-day simulation assuming 20 ppmv H_2O, the final ozone is 22% reduced compared to the 19-day simulation assuming 5 ppmv H_2O. Anderson and Clapp (2018) calculated a similar ozone reduction of 17% in a 14-day simulation and the same potential temperature range of 380 K assuming 20 ppmv H_2O and somewhat higer Cl_y ($\sim$0.2 ppbv) than as used here in the realistic case. In contrast assuming the high Cl_y and NO_y mixing ratios employed by Anderson et al. (2012) in the case of high Cl_y would lead to an ozone loss of 85% (265 ppbv) during the 7-day simulation. This ozone loss would occur in the lower stratosphere.

Borrmann et al. (1996, 1997) and Solomon et al. (1997) conducted a study about the impact of cirrus clouds on chlorine activation and ozone chemistry in the mid-latitudes lowermost stratosphere. They found a significant impact of heterogeneous processes occurring on cirrus clouds for ozone chemistry of the lowermost stratosphere but a minor effect for column ozone. Anderson and Clapp (2018) calculated a fractional loss in the total ozone column of 0.24–0.27% assuming a full Cl_y profile in the altitude range of 12–18 km with a constant water vapour mixing ratio of 20 ppmv and the mixing ratio of Cl_y somewhat higher ($\sim$0.2 ppbv at a potential temperature of 380 K) than in our standard case. However, the simulations of us and Anderson and Clapp (2018) assume a constant high water vapour mixing ratio and neglect mixing with the stratospheric background, which is characterized by much lower water vapour mixing ratios and subsequent dilution of convective uplifted air masses. Ozone loss would only occur in the specific volume of stratospheric air, that is directly affected by the convectively injected additional water. Hence, the ozone loss presented here corresponds to the maximal possible ozone loss for rather realistic convective overshooting conditions.

7 Conclusions

We investigated in detail the ozone loss mechanism at mid-latitudes in the lower stratosphere occurring under enhanced water vapour conditions and the sensitivity of this ozone loss mechanism on a variety of conditions. A CLaMS box-model study was conducted including a standard assumption and a variety of sensitivity cases regarding the chemical initialisation, temperatures and the duration of the simulated period. The assumed standard conditions (155.7 pptv Cl_y, 728.8 pptv NO_y, 197–202 K and an

H_2SO_4 gas phase equivalent of 0.20 ppbv) were determined based on measurements in an H_2O environment showing strongly enhanced H_2O values compared to the stratospheric background during the SEAC^{4}RS aircraft campaign in Texas 2013.

The ozone loss mechanism consists of two phases: The first step is chlorine activation due to the heterogeneous reaction $ClONO_2 + HCl$ (R1), which yields both an increase of ClO_x and a decrease of NO_x. In the second phase, when chlorine is activated, enhanced ClO_x mixing ratios lead to catalytic ozone loss cycles. Our findings show that besides the ClO-Dimer-cycle and the ClO-BrO-cycle, three ozone loss cycles (**C2–C4**) based on the reaction ClO+HO_2 (R13) have to be taken into account. The relevance of the different ozone loss cycles for ozone destruction depends on water vapour, Cl_y and Br_y mixing ratios. Reduced NO_x mixing ratios yield a decreasing chemical net ozone formation in cycle **C1**. This reduced ozone formation at high water vapour mixing ratios in the box-model simulation amounts to around 20% of the ozone destruction in catalytic ozone loss cycles. Furthermore a detailed analysis of chemical processes revealed the occurrence of pathways, which maintain high ClO_x and low NO_x mixing ratios after the chlorine activation step but do not destroy ozone, similar to HCl-null-cycles in the lower stratosphere in Antarctic early spring (Müller et al., 2018).

Focussing on the dependence of chlorine activation on temperature and water vapour mixing ratio, we found that the temperature has to fall below 203 K for chlorine activation to occur at a water vapour mixing ratio of 20 ppmv and Cl_y and NO_y for our standard case. Testing the water vapour dependence of ozone loss along a realistic trajectory that experienced very low temperatures between 197 and 202 K, we observed a water vapour threshold of 10.6 ppmv H_2O, which has to be exceeded for chlorine activation to occur. An ozone loss occurs in these simulations for at least 12 ppmv H_2O. For our assumed standard conditions, a maximum ozone loss of 9% (27 ppbv) was calculated for a water vapour mixing ratio of 20 ppmv. In contrast, a simulation assuming the observed conditions (10.6 ppmv H_2O) yielded ozone formation; but a tripling of background sulphate gas phase equivalent (as it can be reached under geoengineering conditions or volcanic eruptions) is sufficient for a slight ozone loss to occur under these unusually cold conditions. Simulating a high Cl_y case assuming initial Cl_y and NO_y based on the study of Anderson et al. (2012) results in both a lower water vapour threshold of $\sim$8 ppmv and a larger ozone depletion of 85% (265 ppbv) at high water vapour mixing ratios. The model runs described here assume an air parcel moving along the trajectory, which does not mix with neighbouring air masses. In the case of water, mixing would likely reduce the concentration. Because mixing was neglected, the runs discussed here are likely an extreme case, and the ozone loss simulated provides an upper bound.

Considering the duration for which low temperatures and high water vapour mixing ratios have to be maintained to activate chlorine and deplete stratospheric ozone, a chlorine activation time of 24 to 36 hours when the water vapour abundance is close to the water vapour threshold and of 5 h assuming 20 ppmv H_2O was calculated. The water vapour threshold depends strongly on a changing temperature and sulphate content as well as on Cl_y, NO_y and Br_y mixing ratios. The dependence of the water vapour threshold is explained here by focussing on the water dependence of the heterogeneous reactivity (R1) and the balance between heterogeneous chlorine activation (R1, $ClONO_2 + HCl$) and gas phase chlorine deactivation (R12, $Cl + CH_4$).

The ozone loss mechanism was investigated here by conducting box-model simulations along a trajectory, which was calculated based on measurements of enhanced water vapour. Sensitivity and case studies, which cover a range of uncertainties, illustrate the impact of the Cl_y, NO_y, Br_y and H_2O mixing ratios, the temperature, the sulphate gas equivalent and the duration

of the simulated period on the ozone loss process. While the water vapour threshold which has to be exceeded for chlorine activation to occur is mainly determined by the temperature, water vapour mixing ratio and sulphate content, the intensity of ozone loss depends on Cl_y, NO_y, Br_y and the duration of the time period, for which a chlorine activation can be maintained. Our comprehensive sensitivity studies are a basis to assess the impact of enhanced water vapour mixing ratios in the lower mid-latitude stratosphere on ozone under sulphate geoengineering conditions and in a changing climate. However, for the conditions observed during SEAC^{4}RS (in particulary H_2O=10.6 ppmv), we did not simulate any ozone depletion. Global modelling studies are needed to establish whether the mechanism analysed here is of concern for the future.

Code and data availability. The complete SEAC^{4}RS data are availiable at https://www-air.larc.nasa.gov/cgi-bin/ArcView/seac4rs. The CLaMS box model calculations can be requested from Sabine Robrecht (sa.robrecht@fz-juelich.de).

Author contributions. SR, BV and RM developed the concept of the study. SR conducted the box-model simulations. SR, BV, JUG, KR and RM contributed to data interpretation. AR, TT, LC and MK provided in-situ measurements and gave advice on the use of the data. SR wrote the manuscript and designed the figures with contributions from all co-authors.

Appendix A: Maintenance of activated chlorine

In Sec. 3.2.2 chlorine catalysed ozone loss cycles are analysed and the maintainance of activated chlorine is described schematically based on Fig. 6. Here, we describe the pathways yielding the maintainance of activated chlorine and balancing the NO_x mixing ratio in more detail, including all radical balancing reactions. Since the pathway balancing HCl-formation and -destruction is coupled with the pathway balancing HNO_3-formation and -destruction, both are combined here. In total, two pathways are described here, which balance HCl-formation and -destruction as well as HNO_3-formation and -destruction, and which mainly differ in the reaction of the methylperoxy radical (H_3COO + NO, R21, or H_3COO + ClO, R22).
At water vapour mixing ratios slightly higher than the water vapour threshold, H_3COO reacts rather with NO. Hence, pathway

AC1 mainly balances HCl and ClO_x as well as HNO_3 and NO_x.

$$Cl + CH_4 \rightarrow HCl + CH_3 \quad \text{(R12)}$$

$$CH_3 + O_2 \rightarrow H_3COO \quad \text{(AR1)}$$

$$H_3COO + NO \rightarrow NO_2 + H_3CO \quad \text{(R21)}$$

$$H_3CO + O_2 \rightarrow HCHO + HO_2 \quad \text{(AR2)}$$

$$ClO + NO_2 + M \rightarrow ClONO_2 + M \quad \text{(R9)}$$

$$ClONO_2 + HCl \xrightarrow{het.} HNO_3 + Cl_2 \quad \text{(R1)}$$

$$OH + HNO_3 \rightarrow H_2O + NO_3 \quad \text{(R19)}$$

$$Cl_2 + h\nu \rightarrow 2Cl \quad \text{(R10)}$$

$$2 \times (Cl + O_3 \rightarrow ClO + O_2) \quad \text{(R11)}$$

$$NO_2 + h\nu \rightarrow NO + O(^3P) \quad \text{(R7)}$$

$$NO_3 + h\nu \rightarrow NO_2 + O(^3P) \quad \text{(AR3)}$$

$$HO_2 + ClO \rightarrow HOCl + O_2 \quad \text{(R13)}$$

$$HOCl + h\nu \rightarrow OH + Cl \quad \text{(R14)}$$

$$2 \times (O(^3P) + O_2 + M \rightarrow O_3 + M) \quad \text{(AR4)}$$

$$\text{net: } CH_4 + O_2 \rightarrow HCHO + H_2O \quad \textbf{(AC1)}$$

In pathway **AC1**, HCl is formed in R12. The methylradical formed in R12 reacts fastly with oxygen in AR1 yielding a methylperoxy radical H_3COO, which reacts with NO in R21. In reaction R9 $ClONO_2$ is formed, which reacts with HCl heterogeneously in R1 (and thus leads to an HCl depletion). HNO_3 formed in R1 is depleted in R19. These reactions constitute the balance between HCl and HNO_3-formation and -destruction. The reactions R10 and R11 balance the ClO_x-species, R7 and AR3 the NO_x-species, reactions R13 and R14 the HO_x-species and AR4 odd oxygen (O_x). All of these radical reactions are significantly faster than the reactions, which constitute the balance between HCl and HNO_3 formation and destraction. Hence, the net reaction of this pathway is the oxidation of CH_4 to HCHO (formaldehyde).

In cycle **AC1** the H_3COO-radical reacts with NO (R21). As an alternative the H_3COO-radical reacts with ClO (R22) at high

water vapour mixing ratios yielding to cycle **AC2** as balance between HCl and HNO_3 formation and destruction.

$$Cl + CH_4 \rightarrow HCl + CH_3 \quad \text{(R12)}$$

$$CH_3 + O_2 \rightarrow H_3COO \quad \text{(AR1)}$$

$$H_3COO + ClO \rightarrow HCHO + HO_2 + Cl \quad \text{(R22)}$$

$$ClO + NO_2 + M \rightarrow ClONO_2 + M \quad \text{(R9)}$$

$$ClONO_2 + HCl \xrightarrow{het.} HNO_3 + Cl_2 \quad \text{(R1)}$$

$$OH + HNO_3 \rightarrow H_2O + NO_3 \quad \text{(R19)}$$

$$Cl_2 + h\nu \rightarrow 2Cl \quad \text{(R10)}$$

$$3 \times (Cl + O_3 \rightarrow ClO + O_2) \quad \text{(R11)}$$

$$HO_2 + ClO \rightarrow HOCl + O_2 \quad \text{(R13)}$$

$$HOCl + h\nu \rightarrow OH + Cl \quad \text{(R14)}$$

$$O(^3P) + O_2 + M \rightarrow O_3 + M \quad \text{(AR5)}$$

$$\text{net: } CH_4 + 2O_3 \rightarrow HCHO + H_2O + 2O_2 \quad \textbf{(AC2)}$$

The main difference between pathway **AC1** and **AC2** is the reaction of the H_3COO-radical. The reactions R12, AR1, R9, R1 and R19 balance HCl and ClO_x as well as HNO_3 and NO_x. The reactions R10, R11, R13, R14 and AR4 convert the radical species and are very fast. The net reation of this pathway is the oxidation of methane (CH_4) into formaldehyde (HCHO) with a simultaneous ozone destruction. Since the ozone destruction due to the catalytic ozone loss cycles discussed in Sec. 3.2.2 is much faster, the ozone destruction in **AC2** is negligible compared to the ozone loss cycles discussed above.

Appendix B: MACPEX case

The MACPEX case (Mid-latitude airborne Cirrus Properties Experiment) was conducted to complement the results obtained from the standard case as a further example for an event with high stratospheric water vapour based on airborne measurements. In this section, first the model setup for the MACPEX case is described. In a second step, the results of model calculations of the MACPEX case are presented, comprising the chosen trajectory for chemical simulations and the sensitivity of ozone chemistry to various conditions.

B1 Model Setup

Simulations are performed similar to the SEAC^{4}RS case (see. Sec. 2) based on measurements with enhanced water vapour of at least 10 ppmv taken during the MACPEX campaign (Rollins et al., 2014). Chemistry is calculated for single air parcels along

trajectories including diabatic descent. Trajectories are calculated as described in Sec. 2.2. For chemical initialization, important trace gases for ozone chemistry – O_3, Cl_y and NO_y – are initialized based on MACPEX measurements. Ozone and water vapour were measured directly during the aircraft campaign, Cl_y and NO_y are inferred from tracer-tracer relations using N_2O measured on the aircraft employed. The initialization of all further trace gases except of water vapour were taken from the full chemistry 3D-CLaMS simulation (Vogel et al., 2015, 2016) for summer 2012 at the location of the measurement. Chemistry was initialized 7 days before the measurement.

The MACPEX campaign (Rollins et al., 2014) took place during the spring 2011 and was based in Houston, Texas. The water vapour values used here were measured by the Fast In-situ Stratospheric Hygrometer (FISH), which employs the Lyman-α photofragment fluorescence technique (Meyer et al., 2015). MACPEX ozone was measured by the UAS-O_3 instrument (Gao et al., 2012). Initial Cl_y and NO_y were assumed based on tracer-tracer correlations with N_2O that was measured by the Jet Propulsion Laboratory's Aircraft Laser Infrared Absorption Spectrometer (ALIAS) instrument (Webster et al., 1994).

Initial Cl_y and NO_y is calculated based on N_2O tracer-tracer correlations (Grooß et al., 2014, see also App. C) with corrections considering a N_2O increase from 2009 to 2013. Cl_y is determined using the same correlation with CH_4 as for the standard case (see Sec. 2.3). Therefore CH_4 is first calculated using measured N_2O of 320.28 ppbv and a correlation based on measurements from 2009 (Grooß et al., 2014). The increase of stratospheric CH_4 and N_2O is considered as described for the standard case (GHG Bulletin, 2014). First, an increase in N_2O of 1.6 ppbv from 2009 to 2011 is estimated to adjust N_2O. Furthermore calculated CH_4 is adjusted considering a difference between CH_4 in 2000 and 2009 of 0.026 ppm. The annual decrease of Cl_y from 2000 to 2011 is assumed to be 0.8% (WMO, 2014). A summary of the initial values for main tracers assumed in the MACPEX case are given in Table B1. Furthermore sensitivity studies assuming only 80% of initial Cl_y (0.8 Cl_y), 80% of initial NO_y (0.8 NO_y), and an elevated H_2SO_4-background (0.6 ppbv H_2SO_4) are conducted.

B2 Results of MACPEX simulations

During the MACPEX campaign only few cases with enhanced stratospheric water vapour were observed. Here we present an example for a trajectory calculated based on such a case. This trajectory is used to test the sensitivity of lowermost stratospheric ozone in mid-latitudes on the water vapour, Cl_y and NO_y mixing ratio and on an enhancement of stratospheric sulphate.

B2.1 MACPEX Trajectory

The selected trajectory for the MACPEX case is shown in Fig. B1. It refers to a measurement on 11 April 2011 during the MACPEX campaign. In the left panel, a backward trajectory is presented in the range of -7 to 0 days from the time of measurement and a forward trajectory in the range from 0 to 7 days. In the right panel, the location of the measurement is shown by a red square.

The potential temperature level of this trajectory is around 380 K and above the tropopause located at $\sim$350 K, which was deduced from the temperature profile measured during the flight on 11 April 2011. The forward trajectory shows a strongly increasing temperature and pressure level due to a decrease in altitude. Coming from the Western Pacific, this air parcel passes

Table B1. Mixing ratios and sources used for initialization of relevant trace gases for the MACPEX case. Cl_y and NO_y values were determined based on tracer-tracer correlations (see text). Initial mixing ratios of ClO_x species were assumed to be zero.

Species	Value	Source
O_3	283.0 ppbv	UAS-O_3
CH_4	1.68 ppmv	CLaMS-3D
CO	19.0 ppbv	CLaMS-3D
Cl_y	55 pptv	tracer corr.
HCl	52.7 pptv	tracer corr.
$ClONO_2$	2.19 pptv	tracer corr.
NO_y	620 pptv	tracer corr.
HNO_3	390.3 pptv	tracer corr.
NO	114.6 pptv	tracer corr.
NO_2	114.6 pptv	tracer corr.
Br_y	1.2 pptv	CLaMS-3D
H_2O	5–20 ppmv	
H_2SO_4	0.2 ppbv, 0.6 ppbv	

the North American continent briefly. The backward trajectory reaches very low temperatures with a minimum temperature of 191 K. Because of its low temperature, which pushes the occurrence of heterogeneous reactions, the backwards trajectory is chosen to test the sensitivity of lowermost stratospheric ozone to a variety of conditions.

B2.2 Sensitivity studies

Chemical simulations assuming the MACPEX initialization (Tab. B1) and a water vapour mixing ratio varying between 5 and 20 ppmv are perfomed along the MACPEX 7-day backwards trajectory. Final ozone, reached at the end of this simulations, is shown as blue squares in Fig. B2. The water vapour threshold necessary for chlorine activation to occur is reached at 8 ppmv H_2O. It is a lower water vapour mixing ratio than for the SEAC^{4}RS case, beacause of the very low temperatures reached. For the MACPEX trajectory and 8 ppmv H_2O, the time until chlorine is activated takes 63 h from the begin of the trajectory. Because of increasing temperatures (see Fig. B2), chlorine activation can be maintained for 14 h at this water vapour mixing ratio. Hence, no decrease of final ozone can be observed during this simulation. For higher water vapour mixing ratios, chlorine activation is maintained for a longer time and final ozone is reduced comparing with final ozone reached for low water vapour mixing ratios. In general, the decrease in final ozone is much lower for the MACPEX case than for the SEAC^{4}RS case. In the MACPEX initialization, Cl_y is a third of Cl_y in the SEAC^{4}RS initialization. Hence, catalytic ozone loss has lower rates for MACPEX conditions and ozone is less affected by chlorine activation. Even assuming high water vapour of 20 ppmv yields higher final ozone than initial ozone for MACPEX conditions. Although chlorine is activated in the MACPEX case, no net

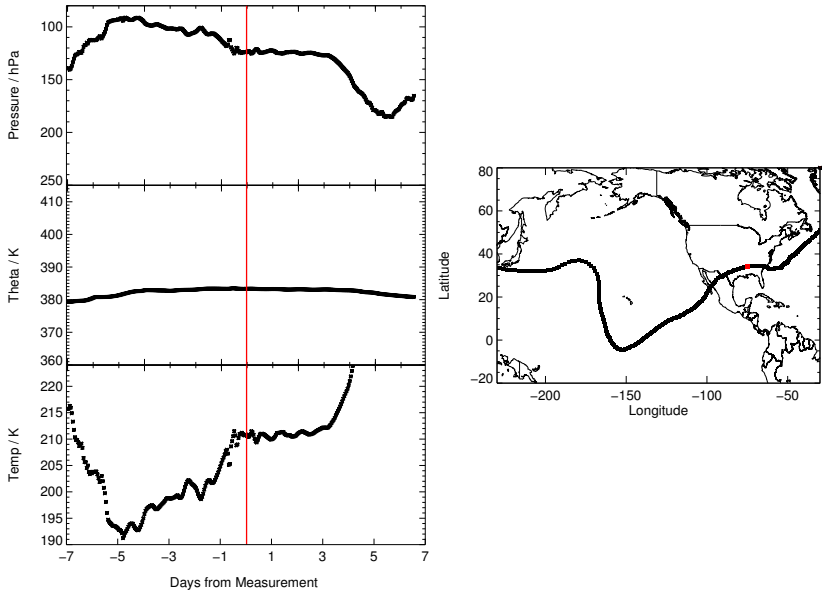

Figure B1. Pressure, potential temperature, temperature and location of the selected trajectory calculated based on measurements with enhanced water vapour during the MACPEX aircraft campaign. The red line (left panels) marks the time of measurement and the red squares (right panels) mark the location of the measurement. Since the tropopause is very low, it is not plotted here. In the right panel, the begin of the trajectory (4. April 2011) is at the left edge of the panel. In the bottom panel (left), the MACPEX trajectory consists of single squares due to a faster movement of the air parcel in that region.

ozone destruction occurs.

The impact of changes in sulphate, Cl_y and NO_y is tested for the MACPEX case, as well. The changes affect the water vapour threshold in the same way as in the SEAC^{4}RS case. An enhacement of sulphate (Fig. 7, left, yellow diamonds), and a reduction of NO_y (green triangles) shifts the water vapour threshold to lower water vapour mixing ratios. A reduction of Cl_y (black circles) shifts it to higher water vapour mixing ratios.

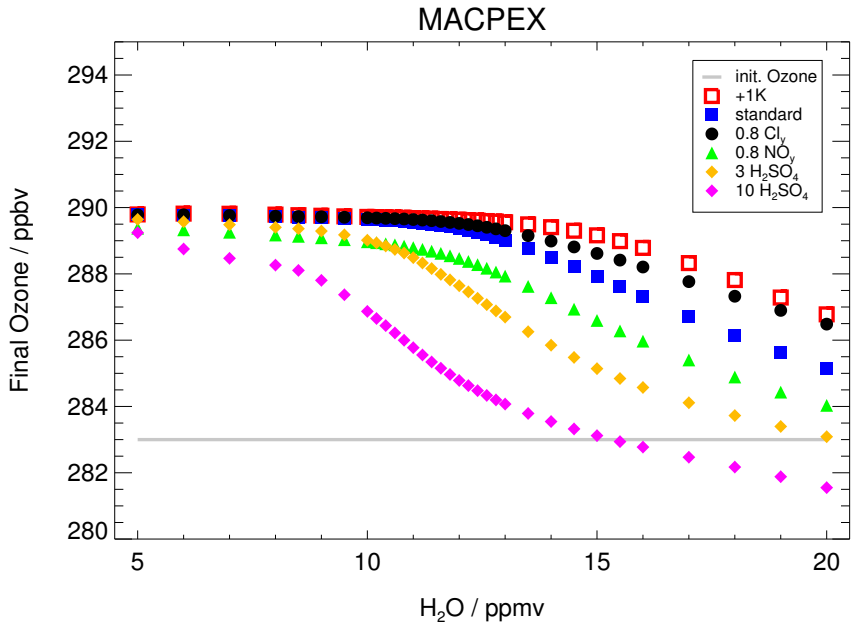

Figure B2. Impact of the water vapour content on the ozone mixing ratio (final ozone) reached at the end of the 7-day simulation along the MACPEX trajectory. The standard case is shown in blue and the initial ozone amount is marked by the grey line. An impact on the final ozone mixing ratios is observable after exceeding a critical threshold in water vapour. This threshold changes with a shift in the temperature (+1K, red), the Cl_y mixing ratio to 0.8 Cl_y (black), the NO_y mixing ratio (0.8 NO_y, green), the sulphate content (3× standard H_2SO_4, yellow, 10× standard H_2SO_4, pink).

Appendix C: Tracer-Tracer Correlations

The mixing ratios of Cl_y and NO_y were initialized based on stratospheric tracer-tracer correlations from Grooß et al. (2014). Cl_y and NO_y were initialized based on a CH_4 measurement during the SEAC^{4}RS aircraft campaign. Initial Cl_y was calculated using the tracer-tracer correlation (Grooß et al., 2014)

$$[Cl_y] = 2.510 + 3.517 \cdot [CH_4] - 3.741 \cdot [CH_4]^2 + 0.4841 \cdot [CH_4]^3 + 0.03042 \cdot [CH_4]^4. \quad \text{(CR1)}$$

The volume mixing ratio of Cl_y ($[Cl_y]$) is here in pptv and the mixing ratio of methane ($[CH_4]$) in ppmv.
To determine NO_y based on the CH_4 measurement, first N2O was calculated through

$$[N_2O] = -124.9 + 311.9 \cdot [CH_4] - 158.1 \cdot [CH_4]^2 + 146.6 \cdot [CH_4]^3 - 43.92 \cdot [CH_4]^4 \quad \text{(CR2)}$$

assuming $[N_2O]$ in ppbv and $[CH_4]$ in ppmv (Grooß et al., 2002). Subsequently NO_y (in ppt) was calculated in a correlation with N_2O.

$$[NO_y] = 11.57 + 0.1235 \cdot [N_2O] - 1.013 \cdot 10^{-3} \cdot [N_2O]^2 + 1.984 \cdot 10^{-6} \cdot [N_2O]^3 - 1.119 \cdot 10^{-9} \cdot [N_2O]^4 \quad \text{(CR3)}$$

In the MACPEX case NO_y and Cl_y were initialized based on N_2O measurements. NO_y was calculated using correlation CR3. Cl_y was calculated using CR1. Therefore first CH_4 (im ppmv) had to be calculated based on a correlation with N_2O (in ppbv) (Grooß et al., 2014).

$$[CH_4] = 0.1917 + 0.01333 \cdot [N_2O] - 8.239 \cdot 10^{-5} \cdot [N_2O]^2 + 2.840 \cdot 10^{-7} \cdot [N_2O]^3 - 3.376 \cdot 10^{-10} \cdot [N_2O]^4 \quad \text{(CR4)}$$

Competing interests. The authors declare that they have no conflict of interest.

Acknowledgements. Our activities were funded by the German Science Foundation (Deutsche Forschungsgemeinschaft, DFG) under the DFG project CE-O_3 in the context of the Priority Program Climate Engineering: Risks, Challenges, Opportunities? (SPP 1689; VO 1276/4-1). We thank the European Centre for Medium-Range Weather Forecasts (ECMWF) for providing ERA-Interim data. We thank the group of Steven Wofsy (Havard University, Department Earth and Planetary Science, Cambridge, MA USA) and Jessica Smith for providing their data measured during the SEAC^{4}RS aircraft campaign. Furthermore, we thank Simone Tilmes for helpful discussions.

References

Anderson, J. G. and Clapp, C. E.: Coupling free radical catalysis, climate change, and human health, Phys. Chem. Chem. Phys., 20, 10 569–10 587, https://doi.org/10.1039/C7CP08331A, 2018.

Anderson, J. G., Wilmouth, D. M., Smith, J. B., and Sayres, D. S.: UV Dosage Levels in Summer: Increased Risk of Ozone Loss from Convectively Injected Water Vapor, Science, 337, 835–839, https://doi.org/10.1126/science.1222978, 2012.

Anderson, J. G., Weisenstein, D. K., Bowman, K. P., Homeyer, C. R., Smith, J. B., Wilmouth, D. M., Sayres, D. S., Klobas, J. E., Leroy, S. S., Dykema, J. A., and Wofsy, S. C.: Stratospheric ozone over the United States in summer linked to observations of convection and temperature via chlorine and bromine catalysis, Proc. Natl. Acad. Sci., 114, E4905–E4913, https://doi.org/10.1073/pnas.1619318114, 2017.

Becker, G., Grooß, J.-U., McKenna, D. S., and Müller, R.: Stratospheric photolysis frequencies: Impact of an improved numerical solution of the radiative transfer equation, J. Atmos. Chem., 37, 217–229, https://doi.org/10.1023/A:1006468926530, 2000.

Berthet, G., Jégou, F., Catoire, V., Krysztofiak, G., Renard, J.-B., Bourassa, A. E., Degenstein, D. A., Brogniez, C., Dorf, M., Kreycy, S., Pfeilsticker, K., Werner, B., Lefèvre, F., Roberts, T. J., Lurton, T., Vignelles, D., Begue, N., Bourgeois, Q., Daugeron, D., Cartiert, M., Robert, C., Gaubicher, B., and Guimbaud, C.: Impact of a moderate volcanic eruption on chemistry in the lower stratosphere: balloon-borne observations and model calculations, Atmos. Chem. Phys., 17, 2229–2253, https://doi.org/10.5194/acp-17-2229-2017, 2017.

Borrmann, S., Solomon, S., Dye, J. E., and Luo, B.: The potential of cirrus clouds for heterogeneous chlorine activation, Geophys. Res. Lett., 23, 2133–2136, https://doi.org/10.1029/96GL01957, 1996.

Borrmann, S., Solomon, S., Avallone, L., Toohey, D., and Baumgardner, D.: On the occurrence of ClO in cirrus clouds and volcanic aerosol in the tropopause region, Geophys. Res. Lett., 24, 2011–2014, https://doi.org/10.1029/97GL02053, 1997.

Brewer, A. W.: Evidence for a world circulation provided by the measurements of helium and water vapour distribution in the stratosphere, Q. J. R. Meteorol. Soc., 75, 351–363, https://doi.org/10.1002/qj.49707532603, 1949.

Brown, P. N., Byrne, G. D., and Hindmarsh, A. C.: VODE: A variable coefficient ODE solver, SIAM J. Sci. Stat. Comput., 10, 1038–1051, https://doi.org/https://doi.org/10.1137/0910062, 1989.

Crutzen, P. J., Müller, R., Brühl, C., and Peter, T.: On the potential importance of the gas phase reaction $CH_3O_2 + ClO \rightarrow ClOO + CH_3O$ and the heterogeneous reaction $HOCl + HCl \rightarrow H_2O + Cl_2$ in "ozone hole" chemistry, Geophys. Res. Lett., 19, 1113–1116, https://doi.org/10.1029/92GL01172, 1992.

Daniel, J. S., Solomon, S., Portmann, R. W., and Garcia, R. R.: Stratospheric ozone destruction: The importance of bromine relative to chlorine, J. Geophys. Res., 104, 23 871–23 880, https://doi.org/10.1029/1999JD900381, 1999.

Dee, D. P., Uppala, S. M., Simmons, A. J., Berrisford, P., Poli, P., Kobayashi, S., Andrae, U., Balmaseda, M. A., Balsamo, G., Bauer, P., Bechtold, P., Beljaars, A. C. M., van de Berg, L., Bidlot, J., Bormann, N., Delsol, C., Dragani, R., Fuentes, M., Geer, A. J., Haimberger, L., Healy, S. B., Hersbach, H., Hólm, E. V., Isaksen, L., Kållberg, P., Köhler, M., Matricardi, M., McNally, A. P., Monge-Sanz, B. M., Morcrette, J.-J., Park, B.-K., Peubey, C., de Rosnay, P., Tavolato, C., Thépaut, J.-N., and Vitart, F.: The ERA-Interim reanalysis: configuration and performance of the data assimilation system, Q. J. R. Meteorol. Soc., 137, 553–597, https://doi.org/10.1002/qj.828, 2011.

Drdla, K. and Müller, R.: Temperature thresholds for chlorine activation and ozone loss in the polar stratosphere, Ann. Geophys., 30, 1055–1073, https://doi.org/10.5194/angeo-30-1055-2012, 2012.

Dykema, J. A., Keith, D. W., Anderson, J. G., and Weisenstein, D.: Stratospheric controlled pertubation experiment: a small-scale experiment to improve understanding of the risks of solar geoengineering, Phil. Trans. R. Soc. A, 372, 1–22, https://doi.org/10.1098/rsta.2014.0059, 2014.

Elrod, M. J., Koch, R. E., Kim, J. E., and Molina, M.: HCl vapour pressures and reaction probabilities for $ClONO_2$+HCl on liquid H_2SO_4-HNO_3-HCl-H_2O solutions, Faraday Discuss., 100, 269–278, 1995.

Gao, R. S., Ballard, J., Watts, L. A., Thornberry, T. D., Ciciora, S. J., McLaughlin, R. J., and Fahey, D. W.: A compact, fast UV photometer for measurement of ozone from research aircraft, Atmos. Meas. Tech., 5, 2201–2210, https://doi.org/10.5194/amt-5-2201-2012, 2012.

GHG Bulletin, ed.: WMO Greenhouse Gas Bulletin, GHG Bulletin No.10, WMO, http://www.wmo.int/pages/prog/arep/gaw/ghg/GHGbulletin.html, 2014.

Grenfell, J. L., Lehmann, R., Mieth, P., Langematz, U., and Steil, B.: Chemical reaction pathways affecting stratospheric and mesospheric ozone, J. Geophys. Res. A, 111, https://doi.org/10.1029/2004JD005713, 2006.

Grooß, J.-U., Günther, G., Konopka, P., Müller, R., McKenna, D. S., Stroh, F., Vogel, B., Engel, A., Müller, M., Hoppel, K., Bevilacqua, R., Richard, E., Webster, C. R., Elkins, J. W., Hurst, D. F., Romashkin, P. A., and Baumgardner, D. G.: Simulation of ozone depletion in spring 2000 with the Chemical Lagrangian Model of the Stratosphere (CLaMS), J. Geophys. Res., 107, 8295, https://doi.org/10.1029/2001JD000456, 2002.

Grooß, J.-U., Brautzsch, K., Pommrich, R., Solomon, S., and Müller, R.: Stratospheric ozone chemistry in the Antarctic: What controls the lowest values that can be reached and their recovery?, Atmos. Chem. Phys., 11, 12 217–12 226, https://doi.org/10.5194/acp-11-12217-2011, 2011.

Grooß, J.-U., Engel, I., Borrmann, S., Frey, W., Günther, G., Hoyle, C. R., Kivi, R., Luo, B. P., Molleker, S., Peter, T., Pitts, M. C., Schlager, H., Stiller, G., Vömel, H., Walker, K. A., and Müller, R.: Nitric acid trihydrate nucleation and denitrification in the Arctic stratosphere, Atmos. Chem. Phys., 14, 1055–1073, https://doi.org/10.5194/acp-14-1055-2014, 2014.

Haagen-Smit, A. H.: Chemistry and physiology of the Los Angeles photochemical smog, Ind. Eng. Chem., 44, 1342–1346, https://doi.org/10.1021/ie50510a045, 1952.

Hanisco, T. F., Moyer, E. J., Weinstock, E. M., Clair, J. M. S., Sayres, D. S., Smith, J. B., Lockwood, R., Anderson, J. G., Dessler, A. E., Keutsch, F. N., Spackman, J. R., Read, W. G., and Bui, T. P.: Observations of deep convective influence on stratospheric water vapor and its isotopic composition, Geophys. Res. Lett., 34, L04814, https://doi.org/10.1029/2006GL027899, 2007.

Hanson, D. R.: Reaction of $ClONO_2$ with H_2O and HCl in sulfuric acid and $HNO_3/H_2SO_4/H_2O$ mixtures, J. Phys. Chem. A, 102, 4794–4807, 1998.

Hanson, D. R. and Ravishankara, A. R.: Reactive Uptake of $ClONO_2$ onto Sulfuric Acid Due to Reaction with HCl and H_2O, J. Phys. Chem., 98, 5728–5735, 1994.

Herman, R. L., Ray, E. A., Rosenlof, K. H., Bedka, K. M., Schwartz, M. J., Read, W. G., Troy, R. F., Chin, K., Christensen, L. E., Fu, D., Stachnik, R. A., Bui, T. P., and Dean-Day, J. M.: Enhanced stratospheric water vapor over the summertime continental United States and the role of overshooting convection, Atmos. Chem. Phys., 17, 6113, https://doi.org/10.5194/acp-17-6113-2017, 2017.

Homeyer, C. R., Pan, L. L., Dorsi, S. W., Avallone, L. M., Weinheimer, A. J., O'Brien, A. S., DiGangi, J. P., Zondlo, M. A., Ryerson, T. B., Diskin, G. S., and Campos, T. L.: Convective transport of water vapor into the lower stratosphere observed during double-tropopause events, J. Geophys. Res., 119, 10 941–10 958, https://doi.org/10.1002/2014JD021485, 2014.

Johnson, D. G., Traub, W. A., Chance, K. V., Jucks, K. W., and Stachnik, R. A.: Estimating the abundance of ClO from simultaneous remote sensing measurements of HO2, OH, and HOCl, Geophys. Res. Lett., 22, 1869–1871, https://doi.org/10.1029/95GL01249, 1995.

Keim, E. R., Fahey, D. W., Negro, L. A. D., Woodbridge, E. L., Gao, R., Wennberg, P. O., Cohen, R. C., Stimpfle, R. M., Kelly, K. K., Hintsa, E. J., Wilson, J. C., Jonsson, H. H., Dye, J. E., Baumgardner, D. G., Kawa, S. R., Salawitch, R. J., Proffitt, M. H., Loewenstein, M., Podolske, J. R., and Chan, K. R.: Observations of large reductions in the NO/NO_y ratio near the mid-latitude tropopause and the role of heterogeneous chemistry, Geophys. Res. Lett., 23, 3223–3226, https://doi.org/10.1029/96GL02593, 1996.

Klooster, S. L. V. and Roebber, P. J.: Surface-Based Convective Potential in the Contiguous United States in a Business-as-Usual Future Climate, J. Climate, 22, 3317–3330, https://doi.org/10.1175/2009JCLI2697.1, 2009.

Koenig, T. K., Volkamer, R., Baidar, S., Dix, B., Wang, S., Anderson, D. C., Salawitch, R. J., Wales, P. A., Cuevas, C. A., Fernandez, R. P., Saiz-Lopez, A., Evans, M. J., Sherwen, T., Jacob, D. J., Schmidt, J., Kinnison, D., Lamarque, J.-F., Apel, E. C., Bresch, J. C., Campos, T., Flocke, F. M., Hall, S. R., Honomichl, S. B., Hornbrook, R., Jensen, J. B., Lueb, R., Montzka, D. D., Pan, L. L., Reeves, J. M., Schauffler, S. M., Ullmann, K., Weinheimer, A. J., Atlas, E. L., Donets, V., Navarro, M. A., Riemer, D., Blake, N. J., Chen, D., Huey, L. G., Tanner, D. J., Hanisco, T. F., and Wolfe, G. M.: BrO and inferred Br_y profiles over the western Pacific: relevance of inorganic bromine sources and a Br_y minimum in the aged tropical tropopause layer, Atmos. Chem. Phys., 17, 15 245–15 270, https://doi.org/10.5194/acp-17-15245-2017, 2017.

Kovalenko, L. J., Jucks, K. W., Salawitch, R. J., Toon, G. C., Blavier, J.-F., Johnson, D. G., Kleinböhl, A., Livesey, N. J., Margitan, J. J., Pickett, H. M., Santee, M. L., Sen, B., Stachnik, R. A., and Waters, J. W.: Observed and modeled HOCl profiles in the midlatitude stratosphere: Implication for ozone loss, Geophys. Res. Lett., 34, https://doi.org/10.1029/2007GL031100, 2007.

LeTexier, H., Solomon, S., and Garcia, R. R.: The role of molecular hydrogen and methane oxidation in the water vapour budget of the stratosphere, Q. J. R. Meteorol. Soc., 114, 281 – 295, https://doi.org/https://doi.org/10.1002/qj.49711448002, 1988.

Luo, B., Krieger, U. K., and Peter, T.: Densities and refractive indices of $H_2SO_4/HNO_3/H_2O$ solutions to stratospheric temperatures, Geophys. Res. Lett., 23, 3707–3710, https://doi.org/10.1029/96GL03581, 1996.

McElroy, M. B., Salawitch, R. J., Wofsy, S. C., and Logan, J. A.: Reductions of Antarctic Ozone due to Synergistic Interactions of Chlorine and Bromine, Nature, 321, 759–762, https://doi.org/10.1038/321759a0, 1986.

McKenna, D. S., Grooß, J.-U., Günther, G., Konopka, P., Müller, R., Carver, G., and Sasano, Y.: A new Chemical Lagrangian Model of the Stratosphere (CLaMS): 2. Formulation of chemistry scheme and initialization, J. Geophys. Res., 107, 4256, https://doi.org/10.1029/2000JD000113, 2002a.

McKenna, D. S., Konopka, P., Grooß, J.-U., Günther, G., Müller, R., Spang, R., Offermann, D., and Orsolini, Y.: A new Chemical Lagrangian Model of the Stratosphere (CLaMS): 1. Formulation of advection and mixing, J. Geophys. Res., 107, 4309, https://doi.org/10.1029/2000JD000114, 2002b.

Meyer, J., Rolf, C., Schiller, C., Rohs, S., Spelten, N., Afchine, A., Zöger, M., Sitnikov, N., Thornberry, T. D., Rollins, A. W., Bozóki, Z., Tátrai, D., Ebert, V., Kühnreich, B., Mackrodt, P., Möhler, O., Saathoff, H., Rosenlof, K. H., and Krämer, M.: Two decades of water vapor measurements with the FISH fluorescence hygrometer: a review, Atmos. Chem. Phys., 15, 8521–8538, https://doi.org/10.5194/acp-15-8521-2015, 2015.

Molina, L. T. and Molina, M. J.: Production of Cl_2O_2 from the self-reaction of the ClO radical, J. Phys. Chem., 91, 433–436, https://doi.org/10.1021/j100286a035, 1987.

Molina, M. J., Tso, T.-L., Molina, L. T., and Wang, F. C.-Y.: Antarctic Stratospheric Chemistry of Chlorine Nitrate, Hydrogen Chloride, and Ice: Release of Active Chlorine, Science, 238, 1253–1257, https://doi.org/10.1126/science.238.4831.1253, 1987.

Müller, R., Grooß, J.-U., Zafar, A., Robrecht, S., and Lehmann, R.: The maintenance of elevated active chlorine levels in the Antarctic lower stratosphere through HCl null cycles, Atmos. Chem. Phys., 18, 2985–2997, https://doi.org/10.5194/acp-18-2985-2018, 2018.

Navarro, M. A., Saiz-Lopez, A., Cuevas, C. A., Fernandez, R. P., Atlas, E., Rodriguez-Lloveras, X., Kinnison, D., Lamarque, J.-F., Tilmes, S., Thornberry, T., Rollins, A., Elkins, J. W., Hintsa, E. J., and Moore, F. L.: Modeling the inorganic bromine partitioning in the tropical tropopause layer over the eastern and western Pacific Ocean, Atmos. Chem. Phys., 17, 9917–9930, https://doi.org/10.5194/acp-17-9917-2017, 2017.

Pitari, G., Visioni, D., Mancini, E., Cionni, I., Di Genova, G., and Gandolfi, I.: Sulfate aerosols from non-explosive volcanoes: chemical-radiative effects in the troposphere and lower stratosphere, Atmosphere, 7, 85, https://doi.org/10.3390/atmos7070085, 2016.

Ploeger, F., Konopka, P., Günther, G., Grooß, J.-U., and Müller, R.: Impact of the vertical velocity scheme on modeling transport across the tropical tropopause layer, J. Geophys. Res., 115, D03301, https://doi.org/10.1029/2009JD012023, 2010.

Poshyvailo, L., Müller, R., Konopka, P., Günther, G., Riese, M., Podglajen, A., and Ploeger, F.: Sensitivities of modelled water vapour in the lower stratosphere: temperature uncertainty, effects of horizontal transport and small-scale mixing, Atmos. Chem. Phys., 18, 8505–8527, https://doi.org/10.5194/acp-18-8505-2018, 2018.

Prather, M. J.: More rapid ozone depletion through the reaction of HOCl with HCl on polar stratospheric clouds, Nature, 355, 534–537, https://doi.org/10.1038/355534a0, 1992.

Randel, W. J., Wu, F., Oltmans, S. J., Rosenlof, K. H., and Nodoluha, G. E.: Interannual Changes of Stratospheric Water Vapor and Correlations with Tropical Tropopause Temperatures, J. Atmos. Sci., 61, 2133–2148, https://doi.org/10.1175/1520-0469(2004)061<2133:ICOSWV>2.0.CO;2, 2004.

Ravishankara, A. R.: Water Vapor in the Lower Stratosphere, Science, 337, 809–810, https://doi.org/10.1126/science.1227004, 2012.

Rohs, S., Schiller, C., Riese, M., Engel, A., Schmidt, U., Wetter, T., Levin, I., Nakazawa, T., and Aoki, S.: Long-term changes of methane and hydrogen in the stratosphere in the period 1978 – 2003 and their impact on the abundance of stratospheric water vapor, J. Geophys. Res., 111, D14315, https://doi.org/10.1029/2005JD006877, 2006.

Rollins, A. W., Thornberry, T. D., Gao, R. S., Smith, J. B., Sayres, D. S., Sargent, M. R., Schiller, C., Krämer, M., Spelten, N., Hurst, D. F., Jordan, A. F., Hall, E. G., Vomel, H., Diskin, G. S., Podolske, J. R., Christensen, L. E., Rosenlof, K. H., and Fahey, D. W.: Evaluation of UT/LS hygrometer accuracy by intercomparison during the NASA MACPEX mission, J. Geophys. Res. A, 119, 1915–1935, https://doi.org/10.1002/2013JD020817, 2014.

Sander, S. P., Friedl, R. R., Barker, J. R., Golden, D. M., Kurylo, M. J., Wine, P. H., Abbatt, J. P. D., Burkholder, J. B., Kolb, C. E., Moortgat, G. K., Huie, R. E., and Orkin, V. L.: Chemical kinetics and photochemical data for use in atmospheric studies, JPL Publication 10-6, 2011.

Schiller, C., Grooß, J.-U., Konopka, P., Plöger, F., Silva dos Santos, F. H., and Spelten, N.: Hydration and dehydration at the tropical tropopause, Atmos. Chem. Phys., 9, 9647–9660, https://doi.org/10.5194/acp-9-9647-2009, 2009.

Schwartz, M. J., Read, W. G., Santee, M. L., Livesesy, N. J., Froidevaux, L., Lamert, A., and Manney, G. L.: Convectively injected water vapor in the North American summer lowermost stratosphere, Geophys. Res. Lett., 40, 2316–2321, https://doi.org/10.1002/grl.50421, 2013.

Shi, Q., Jayne, J. T., Kolb, C. E., Worsnop, D. R., and Davidovits, P.: Kinetic model for reaction of $ClONO_2$ with H_2O and HCl and HOCl with HCl in sulfuric acid solutions, J. Geophys. Res., 106, 24 259–24 274, https://doi.org/10.1029/2000JD000181, 2001.

Smith, J. B., Wilmouth, D. M., Bedka, K. M., Bowman, K. P., Homeyer, C. R., Dykema, J. A., Sargent, M. R., Clapp, C. E., Leroy, S. S., Sayres, D. S., Dean-Day, J. M., Bui, T. P., and Anderson, J. G.: A case study of convectively sourced water vapor observed in the overworld stratosphere over the United States, J. Geophys. Res., 122, 9529–9554, https://doi.org/10.1002/2017JD026831, 2017.

Solomon, S.: Stratospheric ozone depletion: A review of concepts and history, Rev. Geophys., 37, 275–316, https://doi.org/10.1029/1999RG900008, 1999.

Solomon, S., Garcia, R. R., Rowland, F. S., and Wuebbles, D. J.: On the depletion of Antarctic ozone, Nature, 321, 755–758, https://doi.org/10.1038/321755a0, 1986.

Solomon, S., Borrmann, S., Garcia, R. R., Portmann, R., Thomason, L., Poole, L. R., Winker, D., and McCormick, M. P.: Heterogeneous chlorine chemistry in the tropopause region, J. Geophys. Res., 102, 21 411–21 429, 1997.

Solomon, S., Kinnison, D., Garcia, R. R., Bandoro, J., Mills, M., Wilka, C., Neely III, R. R., Schmidt, A., Barnes, J. E., Vernier, J.-P., and Hoepfner, M.: Monsoon circulations and tropical heterogeneous chlorine chemistry, Geophys. Res. Lett., 43, https://doi.org/10.1002/2016GL071778, 2016.

Spang, R., Günther, G., Riese, M., Hoffmann, L., Müller, R., and Griessbach, S.: Satellite observations of cirrus clouds in the Northern Hemisphere lowermost stratosphere, Atmos. Chem. Phys., 15, 927–950, https://doi.org/10.5194/acp-15-927-2015, 2015.

Spang, R., Hoffmann, L., Müller, R., Grooß, J.-U., Tritscher, I., Höpfner, M., Pitts, M., Orr, A., and Riese, M.: A climatology of polar stratospheric cloud composition between 2002 and 2012 based on MIPAS/Envisat observations, Atmos. Chem. Phys., 18, 5089–5113, https://doi.org/10.5194/acp-18-5089-2018, 2018.

Thomason, L. W. and Peter, T., eds.: SPARC Assessment of Stratospheric Aerosol Properties, SPARC Report No. 4, WCRP-124, WMO/TD-No.1295, http://www.atmosp.physics.utoronto.ca/SPARC/index.html, 2006.

Thomason, L. W., Poole, L. R., and Deshler, T.: A global climatoloy of stratospheric aerosol surface area density deduced from Stratospheric Aerosol and Gas Experiment II measurements: 1984-1994, J. Geophys. Res., 102, 8967–8976, https://doi.org/10.1029/96JD02962, 1997.

Thornton, B. F., Toohey, D. W., Tuck, A. F., Elkins, J. W., Kelly, K. K., Hovde, S. J., Richard, E. C., Rosenlof, K. H., Thompson, T. L., Mahoney, M. J., and Wilson, J. C.: Chlorine activation near the midlatitude tropopause, J. Geophys. Res., 112, D18 306, https://doi.org/10.1029/2006JD007640, 2007.

Tilmes, S., Kinnison, D. E., Garcia, R. R., Salawitch, R., Canty, T., Lee-Taylor, J., Madronich, S., and Chance, K.: Impact of very short-lived halogens on stratospheric ozone abundance and UV radiation in a geo-engineered atmosphere, Atmos. Chem. Phys., 12, 10 945–10 955, https://doi.org/10.5194/acp-12-10945-2012, 2012.

Toon, O. B., Maring, H., Dibb, J., Ferrare, R., Jacob, D. J., Jensen, E. J., Luo, Z. J., Mace, G. G., Pan, L. L., Pfister, L., Rosenlof, K. H., Redemann, J., Reid, J. S., Singh, H. B., Thompson, A. M., Yokelson, R., Minnis, P., Chen, G., Jucks, K. W., and Pszenny, A.: Planning, implementation, and scientific goals of the Studies of Emissions and Atmospheric Composition, Clouds and Climate Coupling by Regional Surveys (SEAC4RS) field mission, J. Geophys. Res. A, 121, 4967–5009, https://doi.org/10.1002/2015JD024297, 2016.

Trapp, R. J., Diffenbaugh, N. S., and Gluhovsky, A.: Transient response of severe thunderstorm forcing to elevated greenhouse gas concentrations, Geophys. Res. Lett., 36, https://doi.org/10.1029/2008GL036203, 2009.

Visioni, D., Pitari, G., Aquila, V., Tilmes, S., Cionni, I., Di Genova, G., and Mancini, E.: Sulfate geoengineering impact on methane transport and lifetime: results from the Geoengineering Model Intercomparison Project (GeoMIP), Atmos. Chem. Phys., 17, 11 209–11 226, https://doi.org/10.5194/acp-17-11209-2017, 2017.

Vogel, B., Feck, T., and Grooß, J.-U.: Impact of stratospheric water vapor enhancements caused by CH_4 and H_2 increase on polar ozone loss, J. Geophys. Res., 116, D05301, https://doi.org/10.1029/2010JD014234, 2011.

Vogel, B., Günther, G., Müller, R., Grooß, J.-U., and Riese, M.: Impact of different Asian source regions on the composition of the Asian monsoon anticyclone and of the extratropical lowermost stratosphere, Atmos. Chem. Phys., 15, 13 699–13 716, https://doi.org/10.5194/acp-15-13699-2015, 2015.

Vogel, B., Günther, G., Müller, R., Grooß, J.-U., Afchine, A., Bozem, H., Hoor, P., Krämer, M., Müller, S., Riese, M., Rolf, C., Spelten, N., Stiller, G. P., Ungermann, J., and Zahn, A.: Long-range transport pathways of tropospheric source gases originating in Asia into the

northern lower stratosphere during the Asian monsoon season 2012, Atmos. Chem. Phys., 16, 15 301–15 325, https://doi.org/10.5194/acp-16-15301-2016, 2016.

von Hobe, M., Grooß, J.-U., Günther, G., Konopka, P., Gensch, I., Krämer, M., Spelten, N., Afchine, A., Schiller, C., Ulanovsky, A., Sitnikov, N., Shur, G., Yushkov, V., Ravegnani, F., Cairo, F., Roiger, A., Voigt, C., Schlager, H., Weigel, R., Frey, W., Borrmann, S., Müller, R., and Stroh, F.: Evidence for heterogeneous chlorine activation in the tropical UTLS, Atmos. Chem. Phys., 11, 241–256, https://doi.org/10.5194/acp-11-241-2011, 2011.

Wales, P. A., Salawitch, R. J., Nicely, J. M., Anderson, D. C., Canty, T. P., Baidar, S., Dix, B., Koenig, T. K., Volkamer, R., Chen, D., Huey, L. G., Tanner, D. J., Cuevas, C. A., Fernandez, R. P., Kinnison, D. E., Lamarque, J.-F., Saiz-Lopez, A., Atlas, E. L., Hall, S. R., Navarro, M. A., Pan, L. L., Schauffler, S. M., Stell, M., Tilmes, S., Ullmann, K., Weinheimer, A. J., Akiyoshi, H., Chipperfield, M. P., Deushi, M., Dhomse, S. S., Feng, W., Graf, P., Hossaini, R., Jöckel, P., Mancini, E., Michou, M., Morgenstern, O., Oman, L. D., Pitari, G., Plummer, D. A., Revell, L. E., Rozanov, E., Saint-Martin, D., Schofield, R., Stenke, A., Stone, K. A., Visioni, D., Yamashita, Y., and Zeng, G.: Stratospheric Injection of Brominated Very Short-Lived Substances: Aircraft Observations in the Western Pacific and Representation in Global Models, J. Geophys. Res. A, 123, 5690–5719, https://doi.org/10.1029/2017JD027978, 2018.

Ward, M. K. M. and Rowley, D. M.: Kinetics of the ClO + CH_3O_2 reaction over the temperature range T=250–298 K, Phys. Chem. Chem. Phys., 18, 13 646–13 656, https://doi.org/10.1039/c6cp00724d, 2016.

Webster, C. R., May, R. D., Trimble, C. A., Chave, R. G., and Kendall, J.: Aircraft laser infrared absorption spectrometer (ALIAS) for in situ atmospheric measurements of HCl, N_2O, CH_4, NO_2, and HNO_3, Appl. Opt., 33, 454–472, https://doi.org/10.1364/AO.33.000454, 1994.

Weinstock, E. M., Smith, J. B., Sayres, D. S., Pittman, J. V., Spackman, J. R., Hintsa, E. J., Hanisco, T. F., Moyer, E. J., St Clair, J. M., Sargent, M. R., and Anderson, J. G.: Validation of the Harvard Lyman-α in situ water vapor instrument: Implications for the mechanisms that control stratospheric water vapor, J. Geophys. Res. A, 114, https://doi.org/10.1029/2009JD012427, 2009.

Werner, B., Stutz, J., Spolaor, M., Scalone, L., Raecke, R., Festa, J., Colosimo, S. F., Cheung, R., Tsai, C., Hossaini, R., Chipperfield, M. P., Taverna, G. S., Feng, W., Elkins, J. W., Fahey, D. W., Gao, R.-S., Hintsa, E. J., D., T. T., Lee Moore, F., Navarro, M. A., Atlas, E., Daube, B. C., Pittman, J., Wofsy, S., and Pfeilsticker, K.: Probing the subtropical lowermost stratosphere and the tropical upper troposphere and tropopause layer for inorganic bromine, Atmos. Chem. Phys., 17, 1161–1186, https://doi.org/10.5194/acp-17-1161-2017, 2017.

WMO: Scientific assessment of ozone depletion: 2014, Global Ozone Research and Monitoring Project–Report No. 55, Geneva, Switzerland, 2014.

WMO: Scientific assessment of ozone depletion: 2018, Global Ozone Research and Monitoring Project–Report No. 58, Geneva, Switzerland, 2018.

Zafar, A. M., Müller, R., Grooß, J.-U., Robrecht, S., Vogel, B., and Lehmann, R.: The relevance of reactions of the methyl peroxy radical (CH3O2) and methylhypochlorite (CH3OCl) for Antarctic chlorine activation and ozone loss, Tellus B, 70, 1507 391, https://doi.org/10.1080/16000889.2018.1507391, 2018.

Zhang, R., Jayne, J. T., and Molina, M. J.: Heterogeneous interactions of $ClONO_2$ and HCl with sulfuric acid tetrahydrate: Implications for the stratosphere, J Phys Chem, 98, 867–874, 1994.